

How Sparse Can We Prune A Deep Network: A Fundamental Limit Viewpoint

Qiaozhe Zhang* Ruijie Zhang† Jun Sun‡ Yingzhuang Liu§

Abstract

Network pruning is an effective measure to alleviate the storage and computational burden of deep neural networks arising from its high overparameterization. Thus raises a fundamental question: How sparse can we prune a deep network without sacrifice on the performance? To address this problem, in this work we'll take a first principles approach, i.e. we directly impose the sparsity constraint on the original loss function and then characterize the necessary and sufficient condition of the sparsity (*which turns out to nearly coincide*) by leveraging the notion of *statistical dimension* in convex geometry. Through this fundamental limit, we're able to identify two key factors that determine the pruning ratio limit, i.e., weight magnitude and network flatness. Generally speaking, the flatter the loss landscape or the smaller the weight magnitude, the smaller pruning ratio. In addition, we provide efficient countermeasures to address the challenges in computing the pruning limit, which involves accurate spectrum estimation of a large-scale and non-positive Hessian matrix. Moreover, through the lens of the pruning ratio threshold, we can provide rigorous interpretations on several heuristics in existing pruning algorithms. Extensive experiments are performed that demonstrate that the our theoretical pruning ratio threshold coincides very well with the experiments. All codes are available at: <https://github.com/QiaozheZhang/Global-One-shot-Pruning>

1 Introduction

Deep neural networks (DNNs) have achieved huge success in the past decade, which, however, relies heavily on overparametrization, i.e. the number of parameters are normally several order of magnitudes more than the number of data samples. Though being a key enabler for the striking performance of DNN, overparametrization poses huge burden for computation and storage in practice. It is therefore tempting to ask: 1) Whether can we compress the DNN by a large ratio without sacrifice of performance? 2) What's the fundamental limit of network compressing?

To answer the first question, the main approach is to perform network pruning, which was first introduced by [LDS89]. Network pruning can substantially decrease the number of parameters, thus potentially alleviate the computational and storage burden. The basic idea of network pruning is simple, i.e., to devise metrics to evaluate the significance of parameters and remove the insignificant ones. Various pruning algorithms have been proposed so far: [LDS89, HMD15, HPTD15, LZZ⁺18, ZAP16, WYD⁺18, XWS⁺21, MTK⁺16, LKD⁺16, HLW⁺19] and [HPTD15].

In contrast, our understanding on the second question, i.e., the fundamental limit of network pruning, is unfortunately far less. Some relevant works are: [LFBG21] proposed to characterize the degrees of

*Huazhong University of Science and Technology. qiaozhezhang@hust.edu.cn.

†Huazhong University of Science and Technology. k1seki@hust.edu.cn.

‡Huazhong University of Science and Technology. Author to whom any correspondence should be addressed. juns@hust.edu.cn.

§Huazhong University of Science and Technology. liuyz@hust.edu.cn.

freedom of a DNN by exploiting the framework of Gaussian width. [PCL⁺22] directly applied the above degrees of freedom result to the pruning problem, in the main purpose of unveiling the mechanisms behind the Lottery Thicket Hypothesis (LTH) [FC18]. The lower bound of pruning ratio is briefly mentioned in [PCL⁺22], unfortunately, their predicted lower bound does not match the actual value well, in some cases even with big gap. And there is no discussion on the upper bound in that paper. Moreover, rigorous analysis, detailed interpretation as well as computational issues regarding the pruning limit are all untouched.

Despite the above progress, a systematic of the study on the *fundamental limit* of network pruning is still lacking. To close this gap, we'll take a first principles approach and exploit the powerful framework of the high-dimensional convex geometry. High-level speaking, we'll impose the sparsity constraint directly on the loss function, thus converting the original *pruning limit* problem to a *set intersection* problem, namely, deciding whether the *k-sparse set* intersects with the *loss sublevel set* (the set of weights whose corresponding loss is no larger than the original loss plus a tolerance ϵ), then we can take advantage of the sharp phase transition phenomenon in convex geometry to determine the smallest sparsity.

Intuitively speaking, the larger the loss sublevel set (higher complexity), the smaller the sparse set required for intersection, i.e. the network can be pruned more sparse. To rigorously characterize the complexity of a set, by exploiting the high dimensional property of DNNs, we can exploit the powerful framework of *statistical dimension* and *Gaussian width* in high dimensional convex geometry. Through this geometric perspective, it's possible for us to take advantage of the *concentration* effect [Ver14, Ver20]¹ in the high-dimensional space, thus helping to obtain sharp results regarding the above set intersection problem. In specific, we will exploit the powerful approximate kinematics formula [ALMT14] in convex geometry, which roughly says that for two convex cones, if the sum of their statistical dimension exceeds the ambient dimension, these two cones would intersect with probability 1, otherwise they would intersect with probability 0. It is worthy noting that a sharp phase transition emerge here, thus making a precise characterization of the fundamental limit of network pruning possible.

The key **contributions** of this paper can be summarized as follows:

1. Our work is the first to systematically characterize the fundamental limit of network pruning, whose result coincides well with the experiments. The key message of this fundamental limit are twofold: 1) The smaller the *network flatness* (defined as the trace of the Hessian matrix), the more we can prune the network; 2) The smaller the *weight magnitude*, the more we can prune the network.
2. We provide an efficient *spectrum estimation* algorithm for large-scale Hessian matrices when computing the Gaussian width of a high-dimensional *non-convex* set.
3. We present intuitive explanations on many heuristics utilized in existing pruning algorithms through the lens of our pruning ratio threshold, which include: (a). Why gradually changing the pruning ratio during iterative pruning is preferred. (b). Why there exists significant performance difference in Rare Gems algorithm [SSY⁺22] between using and not using l_2 regularization. (c). Why magnitude pruning might be the optimal pruning strategy.

1.1 Related Work

Pruning Methods: Unstructured pruning involves removing unimportant weights without adhering to some structural constraints. Typical methods in this class include: [HPTD15] presented the train-prune-retrain method, which reduces the storage and computation of neural networks by learning only the significant connections. [YCS17] employed the energy consumption of each layer to determine the pruning order and developed latency tables that employed greed to identify the layers that should be pruned. [GYC16] proposed dynamic network surgery, which reduced network complexity significantly by pruning connections in real time. [FC18] proposed pruning by iteratively removing part of the small weights, and based on Frankle's iterative pruning, [SSY⁺22] introduced l_2 -norm to constrain the magnitude of unimportant parameters during iterative training. We notice that all existing pruning methods are

¹Basically, the concentration effect says that a function of *a large amount* of independent (or weakly dependent) variables tends to concentrate to its expectation value. Notable examples include the Johnson-Lindenstrauss lemma [BSS20] and related results in Compressive Sensing.

heuristic in essence. A systematic exploration of the fundamental limit of network pruning is greatly lacking.

Understanding Neural Networks through Convex Geometry: Convex Geometry is a powerful tool for studying high-dimensional statistical inference [CRPW12] and learning, in specific, the neural networks, considering their high-dimensional nature. In this regard, [LFBG21] studied the training dimension threshold of the network from a geometric point of view by utilizing the Gordon’s Escape theorem, which shows that the network can be trained successfully with less degrees of freedom (DoF) in affine subspace, but the burn-in affine subspace needs a good starting point and also the lottery subspace is greatly affected by the principal components of the entire training trajectory. Therefore, essentially the DoF result in [LFBG21] provides limited knowledge about the pruning ratio threshold, which is exactly the main subject of our work. [PCL⁺22] studied the Lottery Tickets Hypothesis (LTH) pruning by directly applying the above DoF results in [LFBG21] to demonstrate that iteration is needed in LTH and pruning is impacted by the eigenvalues of the loss landscape. The lower bound of pruning ratio is briefly mentioned in their work, however, their predicted lower bound does not match the actual value well, in some cases even with big gap (The main reason is the spectrum estimation error in their adopted SLQ algorithm). Besides, there is no discussion on the upper bound. Moreover, rigorous analysis, detailed interpretation as well as computational issues regarding the pruning limit are all lacking.

2 Problem Setup & Key Tools

To explore the fundamental limit of network pruning, we’ll take the first principles approach. In specific, we directly impose the sparsity constraint on the original loss function, thus the feasibility of pruning can be reduced to determining whether two sets, i.e. *the sublevel set* determined by the Hessian matrix of the loss function and a *k-sparse set* or a subspace intersects. Through this framework, we’re able to leverage powerful tools in high-dimensional convex geometry, such as statistical dimension [ALMT14], Gaussian width [Ver14] and Approximate Kinematics Formula [ALMT14].

Model Setup. Let $\hat{y} = f(\mathbf{w}, \mathbf{x})$ be a deep neural network M with weights $\mathbf{w} \in \mathbb{R}^D$ and inputs $\mathbf{x} \in \mathbb{R}^K$. For a given training data set $\{\mathbf{x}_n, \mathbf{y}_n\}_{n=1}^N$ and loss function ℓ , the empirical loss landscape is defined as $\mathcal{L}(\mathbf{w}) = \frac{1}{N} \sum_{n=1}^N \ell(f(\mathbf{w}, \mathbf{x}_n), \mathbf{y}_n)$. We employ classification as our primary task, where $\mathbf{y} \in \{0, 1\}^k$ with k is the number of classes, and $\ell(f(\mathbf{w}, \mathbf{x}_n), \mathbf{y}_n)$ is the cross-entropy loss.

Pruning Objective. In essence, network pruning can be formulated as the following optimization problem:

$$\min \|\mathbf{w}\|_0 \quad \text{s.t.} \quad \mathcal{L}(\mathbf{w}) \leq \mathcal{L}(\mathbf{w}^*) + \epsilon \quad (2.1)$$

where \mathbf{w} is the optimized weight and \mathbf{w}^* is the original one.

Sparse Network. The weight of the dense network is represented as \mathbf{w}^* , the weight of the k -sparse network, which is obtained by arbitrary pruning principle from \mathbf{w}^* , is denoted as $\mathbf{w}^k = \mathbf{w}^* \odot \mathbf{m}$ with \odot is element wise multiplication and $\|\mathbf{m}\|_0 = k$.

Loss Sublevel Sets. A loss sublevel set of a network is the set of all weights \mathbf{w} that achieve the loss up to $\mathcal{L}(\mathbf{w}^*) + \epsilon$:

$$S(\epsilon) := \{\mathbf{w} \in \mathbb{R}^D : \mathcal{L}(\mathbf{w}) \leq \mathcal{L}(\mathbf{w}^*) + \epsilon\}. \quad (2.2)$$

Feasible k -Sparse Pruning. We call \mathbf{w}^k as a feasible k -sparse pruning if it satisfies:

$$S(\epsilon) \cap \{\mathbf{w}^k\} \neq \emptyset, \quad (2.3)$$

and **the pruning ratio** is defined as $\rho = k/D$.

Below are some key notions and results from high dimensional convex geometry, which are of critical importance to our work.

Definition 2.1 (Convex Cone & Conic Hull). A convex cone $\mathcal{C} \in \mathbb{R}^D$ is a convex set that is positively homogeneous: $\mathcal{C} = \tau\mathcal{C}$ for all $\tau > 0$. The convex conic hull of a sublevel set $S(\epsilon) := \{\mathbf{w} \in \mathbb{R}^D : \mathcal{L}(\mathbf{w}) \leq \mathcal{L}(\mathbf{w}^*) + \epsilon\}$ is for some $\eta > 0$:

$$\mathcal{C}(S(\epsilon)) := \{\mathbf{w} \in \mathbb{R}^D : \mathcal{L}(\eta\mathbf{w}) \leq \mathcal{L}(\mathbf{w}^*) + \epsilon\} \quad (2.4)$$

Statistical dimension is a useful metric to characterize the complexity of a convex cone. Intuitively speaking, the bigger the cone, the larger the statistical dimension, as illustrated in Fig. 1(b).

Definition 2.2 (Statistical Dimension). The statistical dimension $\delta(\mathcal{C})$ of a convex cone \mathcal{C} is:

$$\delta(\mathcal{C}) := \mathbb{E}[\|\Pi_{\mathcal{C}}(\mathbf{g})\|_2^2] \quad (2.5)$$

where $\Pi_{\mathcal{C}}$ is the Euclidean metric projector onto \mathcal{C} and $\mathbf{g} \sim (\mathbf{0}, \mathbf{I}_{D \times D})$ is a standard normal vector.

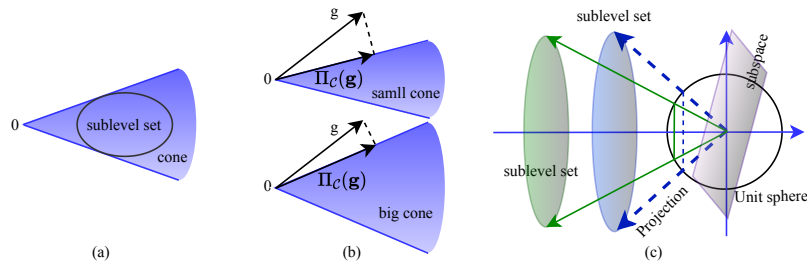


Figure 1: **Panel (a):** Illustration of a convex conic hull of a sublevel set. **Panel (b):** Illustration of the statistical dimension. **Panel (c):** Effect of projection distance on projection size and intersection probability.

To characterize the sufficient and necessary condition of the set (or cone) intersection, the Approximate kinematics Formula [ALMT14] is a powerful and sharp result, which basically says that for two convex cones (or generally, sets), if the sum of their statistical dimension exceeds the ambient dimension, then these two cones would intersect with probability 1, otherwise they would intersect with probability 0.

Theorem 1 (Approximate Kinematics Formula). Let \mathcal{C} be a convex conic hull of a sublevel set $S(\epsilon)$ in \mathbb{R}^D , and draw a random orthogonal basis $\mathbf{Q} \in \mathbb{R}^{D \times D}$. For a k -dimensional subspace W_k , it holds that [ALMT14]:

$$\begin{aligned} \delta(\mathcal{C}) + k \lesssim D &\Rightarrow \mathbb{P}\{\mathcal{C} \cap \mathbf{Q}W_k = \{\mathbf{0}\}\} \approx 1 \\ \delta(\mathcal{C}) + k \gtrsim D &\Rightarrow \mathbb{P}\{\mathcal{C} \cap \mathbf{Q}W_k = \{\mathbf{0}\}\} \approx 0 \end{aligned}$$

Theorem 1 indicates that when $k \lesssim D - \delta(\mathcal{C})$, the k -dimensional subspace and the cone do not share a ray.

3 Lower Bound of Pruning Ratio

In this section, we aim to characterize the lower bound of the pruning ratio, i.e. when the pruning ratio falls below a threshold, it's impossible to keep the generalization performance nearly unaffected. To establish the impossibility result, we'll leverage the powerful Approximate Kinematics Formula as detailed in Theorem 1.

3.1 Network Pruning As Set Intersection Problem

Sparse Set Consider a weight \mathbf{w}^k of a k -sparse network (pruned by arbitrary pruning algorithm), we define a k -sparse set $W_k = \{\mathbf{s}^k + \mathbf{w}^k : \mathbf{s}^k \in S_k\}$, where the position of 0 elements in the vector from S_k is the same as \mathbf{w}^k . Here, S_k is a subset of a vector space that is closed under addition and scalar multiplication, i.e. S_k is a **subspace**. If W_k and $S(\epsilon)$ do not intersect, $\mathbf{w}^k \notin S(\epsilon)$, there is no k -sparse solution.

In order to apply Theorem 1, we translate W_k to the origin and perform a simultaneous translation of $S(\epsilon)$ in the same direction and distance, and we denote the translated $S(\epsilon)$ as $S_{\mathbf{w}^k}$. The infeasible k -sparse solutions can be formulated as: $S_{\mathbf{w}^k} \cap S_k = \emptyset$, since S_k is a subspace centered at the origin, $S_{\mathbf{w}^k} \cap S_k = \emptyset$ and $\mathcal{C}(S_{\mathbf{w}^k}) \cap S_k = \emptyset$ are equivalent. Therefore, we can utilize the statistical dimension in theorem 1 to determine the threshold where d -sparse solutions do not exist. Next, we will introduce the Gaussian width for calculating the statistical dimension of $\mathcal{C}(S_{\mathbf{w}^k})$.

Definition 3.1 (Gaussian Width). *The gaussian width of a subset $S \in \mathbb{R}^D$ is given by:*

$$w(S) = \frac{1}{2} \mathbb{E} \sup_{\mathbf{x}, \mathbf{y} \in S} \langle \mathbf{g}, \mathbf{x} - \mathbf{y} \rangle, \mathbf{g} \sim \mathcal{N}(\mathbf{0}, \mathbf{I}_{D \times D}). \quad (3.1)$$

[ALMT14] indicates that the Gaussian width of a spherical convex set is comparable with the statistical dimension of the cone generated by the set:

Theorem 2. *Given a unit sphere $\mathbb{S}^{D-1} := \{\mathbf{x} \in \mathbb{R}^D : \|\mathbf{x}\| = 1\}$, let \mathcal{C} be a convex cone in \mathbb{R}^D , then:*

$$w(\mathcal{C} \cap \mathbb{S}^{D-1})^2 \leq \delta(\mathcal{C}) \leq w(\mathcal{C} \cap \mathbb{S}^{D-1})^2 + 1 \quad (3.2)$$

As theorem 2 requires the set to be a spherical convex set, for using Gaussian width as a proxy for statistical dimension, we need project the sublevel set $S_{\mathbf{w}^k}$ onto the surface of the unit sphere centered at origin. The projection of $S_{\mathbf{w}^k}$ is defined as:

$$p(S_{\mathbf{w}^k}) = \{(\mathbf{x} - \mathbf{w}^k) / \|\mathbf{x} - \mathbf{w}^k\|_2, \mathbf{x} \in S\} \quad (3.3)$$

Consider two manifolds with equal width, it can be observed that as the distance from the sphere increases, the projected part on the sphere decreases, and the Gaussian width of the spherical convex set also decreases, leading to the cone becoming smaller, thus with a reduced probability of intersection with the subspace. This relationship is visually depicted in Figure 1(c). By invoking theorem 1 in the projection setting, the lower bound of pruning ratio is expressed as:

Theorem 3 (Lower Bound of Pruning Ratio). *Let \mathcal{C} be a convex conic hull of a sublevel set $S_{\mathbf{w}^k}$ in \mathbb{R}^D . There does not exist a k -sparse weight vector with probability 1, if the following holds:*

$$w(p(S_{\mathbf{w}^k}))^2 + k \lesssim D$$

This theorem tells us that when the dimension of the sub-network is lower than $k_L = D - w(p(S_{\mathbf{w}^k}))^2$, the subspace will not intersect with $S_{\mathbf{w}^k}$, ie., no k_L -sparse solution can be found. Therefore, the lower bound of the pruning ratio of the network M can be expressed as:

$$\rho_L = \frac{D - w(p_{\mathbf{w}^k}(S))^2}{D} = 1 - \frac{w(p_{\mathbf{w}^k}(S))^2}{D}. \quad (3.4)$$

3.2 Characterization of The Sublevel Set

Consider a well-trained deep neural network model M^* with weights \mathbf{w}^* and an arbitrary loss function $\mathcal{L}(\mathbf{w})$, where \mathbf{w} lies in a small neighborhood of \mathbf{w}^* . Perform a Taylor expansion of $\mathcal{L}(\mathbf{w})$ at \mathbf{w}^* :

$$\mathcal{L}(\mathbf{w}) = \mathcal{L}(\mathbf{w}^*) + (\mathbf{w} - \mathbf{w}^*)\mathbf{G} + \frac{1}{2}(\mathbf{w} - \mathbf{w}^*)^T \mathbf{H}(\mathbf{w} - \mathbf{w}^*) + \Delta. \quad (3.5)$$

where \mathbf{G} and \mathbf{H} denote the first and second derivatives of $\mathcal{L}(\mathbf{w})$ with respect to the model parameters \mathbf{w} , and Δ represents the higher order terms in the Taylor expansion which can be ignored. For a well-trained deep neural network model, the first derivatives of $\mathcal{L}(\mathbf{w})$ satisfy $\mathbf{G} = \mathbf{0}$ and the second derivatives \mathbf{H} is a positive definite matrix. Consequently, the loss sublevel set $S(\epsilon)$ can be expressed as:

$$S(\epsilon, \mathbf{w}^*) = \{\hat{\mathbf{w}} \in \mathbb{R}^D : \frac{1}{2} \hat{\mathbf{w}}^T \mathbf{H} \hat{\mathbf{w}} \leq \epsilon\} \quad (3.6)$$

where $\hat{\mathbf{w}} = \mathbf{w} - \mathbf{w}^*$. Due to the positive definiteness property of \mathbf{H} , $S(\epsilon, \mathbf{w}^*)$ forms an ellipsoid, and the proof regarding the ellipsoid can be found in Appendix C.1.

3.3 Gaussian Width of the Ellipsoid

We leverage tools in high-dimensional probability, especially the concentration of measure, which enables us to present a rather precise expression for the Gaussian width of the high-dimensional ellipsoid.

Lemma 3.2. *Give an ellipsoid $S(\epsilon)$ defined by a quadratic form: $S(\epsilon) := \{\mathbf{w} \in \mathbb{R}^D : \frac{1}{2} \mathbf{w}^T \mathbf{H} \mathbf{w} \leq \epsilon\}$ where $\mathbf{H} \in \mathbb{R}^{D \times D}$ is a symmetric, positive definite Hessian matrix. Loss sublevel set $S(\epsilon)$ defined by \mathbf{H} is an ellipsoidal body with the Gaussian width:*

$$w(S(\epsilon)) \approx (2\epsilon \text{Tr}(\mathbf{H}^{-1}))^{1/2} = \left(\sum_{i=1}^D r_i^2 \right)^{1/2} \quad (3.7)$$

where $r_i = \sqrt{2\epsilon/\lambda_i}$ is the radius of ellipsoidal body and λ_i is the i -th eigenvalue of \mathbf{H} .

The proof of Lemma 3.2 is in Appendix C.1. The Gaussian width of an ellipsoid demonstrated by [LFBG21] is $[(\sqrt{\frac{2}{\pi}} (\sum_{i=1}^D r_i^2)^{1/2}, (\sum_{i=1}^D r_i^2)^{1/2})]$, the most notable **difference** is that our established Gaussian width $(\sum_{i=1}^D r_i^2)^{1/2}$ is not represented as an interval but as a value. Under the projection settings, the squared radius r_i^2 will be modified to $\frac{r_i^2}{\|\mathbf{w}^* - \mathbf{w}^k\|_2^2 + r_i^2}$. Such modification can be found in [LFBG21].

Therefore, the projected Gaussian width of $S(\epsilon, \mathbf{w}^*)$ defined in Eq.(3.6) becomes:

$$w(p_{\mathbf{w}^k}(S)) = \left(\sum_{i=1}^D \frac{r_i^2}{\|\mathbf{w}^* - \mathbf{w}^k\|_2^2 + r_i^2} \right)^{1/2} \quad (3.8)$$

3.4 Lower Bound of Pruning Ratio

According to Eq.(3.4), we have the lower bound of the pruning ratio as follows:

Corollary 3.3. *Given a well-trained deep neural network model M with trained weight $\mathbf{w}^* \in \mathbb{R}^D$ and arbitrary loss function $\mathcal{L}(\mathbf{w})$, for a k -sparse pruned weight \mathbf{w}^k , the lower bound of pruning ratio of model M is:*

$$\rho_L = 1 - \frac{1}{D} \sum_{i=1}^D \frac{r_i^2}{\|\mathbf{w}^* - \mathbf{w}^k\|_2^2 + r_i^2}. \quad (3.9)$$

where $r_i = \sqrt{2\epsilon/\lambda_i}$ and λ_i is the eigenvalue of the Hessian matrix of the loss function $\mathcal{L}(\mathbf{w})$ with respect to \mathbf{w} .

3.5 Pruning Ratio vs Magnitude & Flatness

It is evident from Eq.3.9 that for a given trained network (whose spectrum of Hessian matrix is fixed), to obtain the lowest possible value of the lower bound, we just need to minimize $\|\mathbf{w}^* - \mathbf{w}^k\|_2$, i.e. the sum of magnitudes of the pruned parameters. Therefore, the commonly-used magnitude-based pruning algorithms get justified, and moreover, it inspires us to develop a one-shot magnitude pruning algorithm in Section 5, whose performance is better than all existing algorithms as far as we know.

Besides the above discussed magnitude of pruned sub-vector, we identify another important factor that determine the pruning ratio, i.e. the *network flatness*, which describes the flatness of the loss landscape around the minima and is defined as the trace of Hessian matrix $\text{Tr}(\mathbf{H})$ [PKA⁺21] and [GLC⁺23].

Lemma 3.4 (Pruning Ratio vs. Flatness). *Given a well-trained neural network $f(\mathbf{w}, \mathbf{x})$, where \mathbf{w} is the parameters and the \mathbf{x} is the input. The lower bound of pruning ratio and the flatness obeys:*

$$\rho_L \leq 1 - \frac{\epsilon D}{\|\mathbf{w}^* - \mathbf{w}^k\|_2^2 \text{Tr}(\mathbf{H}) + \epsilon D} \quad (3.10)$$

where \mathbf{H} is the hessian matrix of $f(\mathbf{w})$ w.r.t. \mathbf{w} , and $r_i = \epsilon/\lambda_i$ where λ_i is the eigenvalue of \mathbf{H} .

Lemma 3.4 can be obtained by utilizing Cauchy–Schwarz Inequality, which can be found in Appendix D.3. It can be seen from Lemma 3.4 that the lower bound of the network pruning ratio is highly dependent on by the flatness of the network, i.e. flatter networks imply more sparsity. This can be a valuable guideline for both training and pruning the networks.

4 Upper Bound of Pruning Ratio

In order to establish the upper bound of the pruning ratio, we need to prove that there exists an k -sparse weight vector intersects with the loss sub-level set.

For a given trained weight \mathbf{w}^* , we split it into two parts, i.e. the unpruned subvector, $\mathbf{w}^1 = [\mathbf{w}_1^*, \mathbf{w}_2^*, \dots, \mathbf{w}_k^*]$ and pruned one $\mathbf{w}^2 = [\mathbf{w}_{k+1}^*, \mathbf{w}_{k+2}^*, \dots, \mathbf{w}_D^*]$. By fixing \mathbf{w}^1 , the loss sublevel set can be reformulated as:

$$S(\mathbf{w}^2) = \{\mathbf{w}^2 \in \mathbb{R}^{D-k} : \mathcal{L}([\mathbf{w}^1, \mathbf{w}^2]) \leq \mathcal{L}(\mathbf{w}^*) + \epsilon\} \quad (4.1)$$

In order to prove the existence of a k -sparse weight vector \mathbf{w}^k , we just need to show that the all-zero vector is in $S(\mathbf{w}^2)$. To that end, we'll take advantage of the sufficient part of the approximate kinematics formula (Theorem 1) to show that it suffices to make the statistical dimension of the projected cone of $S(\mathbf{w}^2)$ is full, i.e. $D - k$. Thus we can obtain the upper bound of the size of unpruned parameters, i.e. k .

Specifically, by invoking the sufficient part of Theorem 1, the upper bound of the pruning ratio by a given pruning strategy is as follows:

Theorem 4 (Upper Bound of Pruning Ratio). *Given a sublevel set $S_{\mathbf{w}^2}$ in \mathbb{R}^{D-k} . To ensure that the all-zero vector $\mathbf{w}^2 \in \mathbb{R}^{D-k}$ contained in $S_{\mathbf{w}^2}$, it suffices that:*

$$w(p(S_{\mathbf{w}^2}))^2 \gtrsim D - k.$$

The Gaussian width of projected $S(\mathbf{w}^2)$ can be easily obtained by employing Lemma 3.2, i.e. $w(p(S_{\mathbf{w}^2}))^2 = \sum_i^{D-k} \frac{\tilde{r}_i^2}{\|\mathbf{w}^* - \mathbf{w}^k\|_2^2 + \tilde{r}_i^2}$, where $\tilde{r}_i = \sqrt{2\epsilon/\tilde{\lambda}_i}$, $\tilde{\lambda}_i$ is the eigenvalue of the hessian matrix of $\mathcal{L}([\mathbf{w}^1, \mathbf{w}^2])$ w.r.t. to \mathbf{w}^2 and the fact that $\|\mathbf{w}^* - \mathbf{w}^k\|_2 = \|\mathbf{w}^2\|_2$ is used.

Correspondingly, the upper bound of the pruning ratio can be expressed as:

$$\rho_U = 1 - \frac{w(p(S_{\mathbf{w}^2}))^2}{D} = 1 - \frac{1}{D} \sum_i^{D-k} \frac{\tilde{r}_i^2}{\|\mathbf{w}^* - \mathbf{w}^k\|_2^2 + \tilde{r}_i^2}.$$

5 Achievable Scheme & Computational Issues

We have established the lower bound and upper bound of pruning ratio by leveraging the approximate kinematic formula in convex geometry [ALMT14]. To proceed, we will demonstrate that our obtained bounds are tight in the sense that we can devise an achievable pruning algorithm whose corresponding

upper bound is quite close to the lowest possible value of the lower bound. As argued in Corollary 3.3, the magnitude pruning, which removes all the smallest $D - k$ weights, will result in the lowest pruning ratio lower bound. Inspired by this result, we’ll focus on the magnitude pruning methods in order to approach the lower bound in the sequel.

For the lower bound part, we need to address several challenges regarding the computation of the Gaussian width of a high-dimensional deformed ellipsoid, which involves tackling the *non-positiveness* of the Hessian matrix as well as the *spectrum estimation* of a large-scale Hessian matrix.

For the upper bound part, we’ll focus on a *relaxed* version of Eq.2.1 by introducing the l_1 regularization term, for the sake of computational complexity. Then we’ll employ the *one-shot* magnitude pruning to compress the network.

5.1 Computational Challenges & Countermeasures

To compute the lower bound of the pruning ratio, we need to address the following two challenges:

1). (*Gaussian Width of the Deformed Ellipsoid*) In practice, it is usually hard for the network to converge to the exact minima, thus leading to a non-positive definite Hessian matrix. In other words, the ideal ellipsoid gets deformed due to the existence of negative eigenvalues. Determining the Gaussian width of the deformed ellipsoid is a challenging task. To address this problem, we resort to convexifying (i.e. taking the convex hull of) the deformed ellipsoid and then calculating the Gaussian width of the latter instead. The proof that the convexifying procedure has no impact on the Gaussian width is presented in Appendix B.

2). (*Improved Spectrum Estimation*) Neural networks often exhibit a very significant number of zero-valued or vanishingly small eigenvalues in their Hessian matrices. It’s hard for the spectrum estimation algorithm SLQ(Stochastic Lanczos Quadrature) proposed by [YGKM20] to obtain accurate estimation of these small eigenvalues. To address this issue, we propose to enhance the existing large-scale spectrum estimation algorithms by a key modification, i.e, to estimate the number of these exceptionally small eigenvalues by employing Hessian matrix sampling. A comprehensive description of the algorithm and its numerical performance are presented in Appendix B.

5.2 Achievable Scheme: l_1 Regularization & One-shot Magnitude Pruning

Inspired by the lower bound as well as upper bound of the pruning ratio, in which the magnitude of pruning parameters plays a key role, it’s sensible to focus on the magnitude pruning methods. On the other hand, to find exact solutions of our original problem for the best pruning, i.e. Eq. 2.1, is obviously very hard due to the existence of l_0 norm. To make it feasible, it’s natural to perform a convex relaxation of l_0 norm, namely, by employing l_1 regularization instead. Aside from the computational advantage of this relaxation, it is worthy noting that l_1 regularization provides extra two-fold benefits: 1) a large portion of eigenvalues of the trained Hessian matrix are zero-valued or of quite small value, thus rendering the calculation of the pruning limit more accurately and fast. 2) a large portion of trained weights are of quite small value, thus making the lower bound and upper bound very close. Detailed statistics about the eigenvalues and magnitudes can be found in Figure 6.

Specifically, by utilizing the Lagrange formulation and convex relaxation of l_0 norm, the fundamental pruning objective in Eq.2.1 can be reformulated as:

$$\min \mathcal{L}(\mathbf{w}) + \lambda \|\mathbf{w}\|_1 \tag{5.1}$$

After training with this relaxed objective, the network weights will be pruned based on magnitudes *in one time*, rather than in an iterative way as in [HPTD15, FC18, SSY⁺22]. The performance of the above described pruning scheme (termed as “ *l_1 regularized one-shot magnitude pruning*”) can be found

in Section 6.

The above-mentioned "zero-dominating" property due to l_1 regularization is supported in Figure 2(b), where it can be seen that the majority of weights are extremely small.

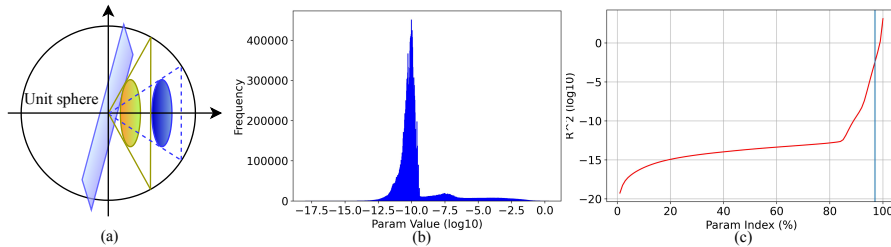


Figure 2: Effect of extremely small projection distance on projection size and intersection probability and statistics of ResNet50 on TinyImagenet. Statistics regarding all experiments can be found in Appendix E.

The above "zero-domination" property turns out to be critical for our proposed pruning scheme to nearly achieve the fundamental limit (lower bound) of the pruning ratio. As illustrated in 2(c), where the curve represents $\|\mathbf{w}^2\|_2^2$, i.e. the l_2 norm of the $D - k$ smallest weights w.r.t. k/D . Besides, the vertical line represents ρ_L , the lower bound of the pruning ratio predicted in Section 3. When $k = D\rho_L$, the curve and the line will intersect as shown in Figure 2(c). Mathematically, the upper bound for the pruning ratio can be approximated as follows:

$$\rho_U = 1 - \frac{1}{D} \sum_{i=1}^{D-k} \frac{\tilde{r}_i^2}{\|\mathbf{w}^2\|_2^2 + \tilde{r}_i^2} \approx 1 - \frac{1}{D} \sum_{i=1}^{D-k} \frac{\tilde{r}_i^2}{\tilde{r}_i^2} = \frac{k}{D} = \rho_L$$

It can be seen from the above demonstration that the upper bound corresponding to our proposed pruning scheme nearly *coincides* the (lowest possible) lower bound! This is to say we have established the fundamental limit of the pruning ratio. To provide further validation of the above claim, we executed the experiments five times across eight tasks and reported the differences between the upper bound and lower bound, denoted as Δ , as is summarized in Table 1.

Table 1: The Difference Between Lower Bound and Upper Bound of Pruning Ratio. C100 for CIFAR100 and TIN for TinyImagenet.

CIFAR10	FC5	FC12	Alexnet	VGG16
$\Delta(\%)$	0.17±0.05	0.05±0.03	0.02±0.01	0.01±0.00
ResNet	18 on C100	50 on C100	18 on TIN	50 on TIN
$\Delta(\%)$	0.12±0.05	0.11±0.09	0.09±0.01	0.27±0.22

6 Experiments

In this section, we experimentally validate our pruning method and lower bound on network pruning using the Approximate Kinematics Formula.

Tasks. We evaluate the pruning algorithm and pruning ratio threshold on: Full-Connect-5(FC5), Full-Connect-12(FC12), AlexNet [KSH17] and VGG16 [SZ14] on CIFAR10 [KH⁺09], ResNet18 and ResNet50 [HZRS16] on CIFAR100 and TinyImageNet [LY15]. We make use of theoretical principles to anticipate the pruning ratio limit of the network, followed by an evaluation of the sparse sub-networks performance at different sparse ratios on test data. Specifically, we calculate accuracy and loss metrics to quantify their performance. Finally, we compare the predicted lower bound on the pruning ratio with the actual pruning ratio and evaluate whether they match. Detailed descriptions of datasets, networks, hyper-parameters and eigenspectrum adjustment can be found in Section A of the Appendix.

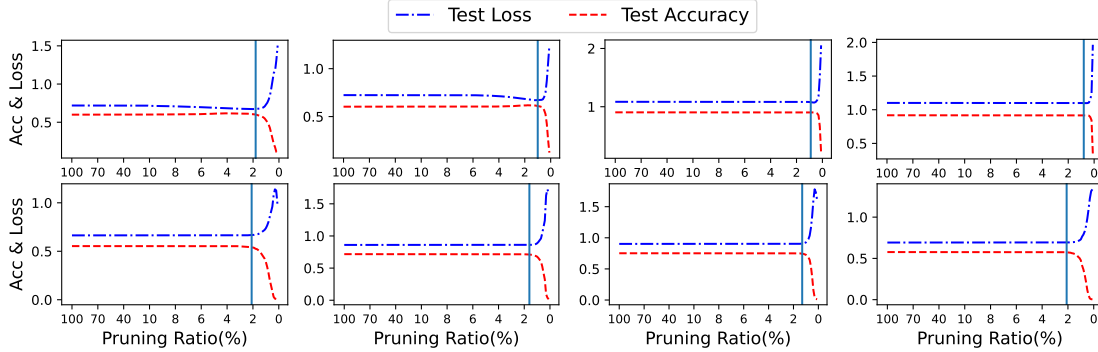


Figure 3: We assessed the influence of sparsity on loss and test accuracy using the test dataset, and we marked the theoretical pruning ratio with vertical lines. The first row, from left to right, corresponds to FC5, FC12, AlexNet, and VGG16. The second row, from left to right, corresponds to ResNet18 and ResNet50 on CIFAR100, as well as ResNet18 and ResNet50 on TinyImagenet. The figures demonstrate that our theory predicts the critical pruning points quite accurately.

6.1 Validation of Pruning Lower Bound:

We validated our prediction results on several tasks for the lower bound of network pruning. The images generated during the experimental process, such as the statistical plots of Hessian matrix row l_1 norm, can be found in Appendix B. Figure 3 shows the sparsity-accuracy trade-off in all tasks and provides strong evidence of the high redundancy of deep neural networks. The theoretical lower bound we derive matches well with the practical pruning ratio threshold.

6.2 Prediction Performance

The numerical comparison between the predicted pruned weights ratio and the actual value is shown in Table 2. The results in Table 2 exhibit a high degree of agreement between the predicted and actual values which demonstrate that our theoretical predictions effectively estimate the network pruning ratio threshold.

Table 2: Comparison between Prediction of Pruned Parameters Ratio and Actual Values. Abbreviations: C10 for CIFAR10, C100 for CIFAR100 and TIN for TinyImagenet.

Dataset	Model	Theo. Value(%)	Actual Value(%)	Δ (%)
C10	FC5	97.9 \pm 0.25	98.3 \pm 0.12	-0.40 \pm 0.35
	FC12	99.0 \pm 0.30	99.2 \pm 0.06	-0.15 \pm 0.26
	AlexNet	99.1 \pm 0.00	99.2 \pm 0.08	-0.14 \pm 0.08
	VGG16	99.2 \pm 0.06	99.2 \pm 0.06	0.04 \pm 0.08
C100	ResNet18	98.5 \pm 0.05	98.0 \pm 0.13	0.54 \pm 0.15
	ResNet50	98.1 \pm 0.05	97.9 \pm 0.16	0.28 \pm 0.19
TIN	ResNet18	96.1 \pm 0.82	95.7 \pm 0.38	0.46 \pm 0.71
	ResNet50	97.4 \pm 0.24	97.1 \pm 0.33	0.36 \pm 0.10

6.3 Comparison of Pruning Algorithms

We validated l_1 -regularization based global one-shot pruning algorithm(GOP) against four baselines: dense weight training and three pruning algorithms: (i) Rare Gems(RG) proposed by [SSY⁺22], (ii) Lottery Tickets Hypothesis(LTH) donated by [FC18], (iii) Smart-Ratio (SR) which is the random pruning method proposed by [SCC⁺20]. Table 3 shows the pruning performance of the above algorithms, our pruning algorithm is better performing than other algorithms.

Table 3: Performance comparison of various pruning algorithms.

Dataset	Model	Dense Acc (%)	Sparsity (%)	Test Acc (%)@top-1			
				GOP(ours)	RG	LTH	SR
CIFAR10	FC5	55.3±0.62	1.7	59.96±0.45	58.76±0.15	38.71±2.25	-
	FC12	55.5±0.26	1.0	60.84±0.21	54.96±0.28	10.00±0.00	-
	AlexNet	89.60±0.31	0.7	90.55±0.04	85.55±0.11	21.65±2.63	10.00±0.00
	VGG16	90.73±0.22	0.6	91.66±0.08	87.66±0.11	86.59±0.21	10.00±0.00
CIFAR100	ResNet18	72.19±0.23	1.9	71.82±0.09	67.52±0.30	64.42±0.20	66.50±0.24
	ResNet50	74.07±0.43	2.0	75.22±0.11	70.96±0.23	61.17±0.45	66.99±0.21
TinyImageNet	ResNet18	52.92±0.13	4.2	55.42±0.02	37.14±0.20	55.02±0.27	53.28±0.25
	ResNet50	56.45±0.17	2.9	57.49±0.01	36.78±0.13	49.35±1.27	53.65±0.34

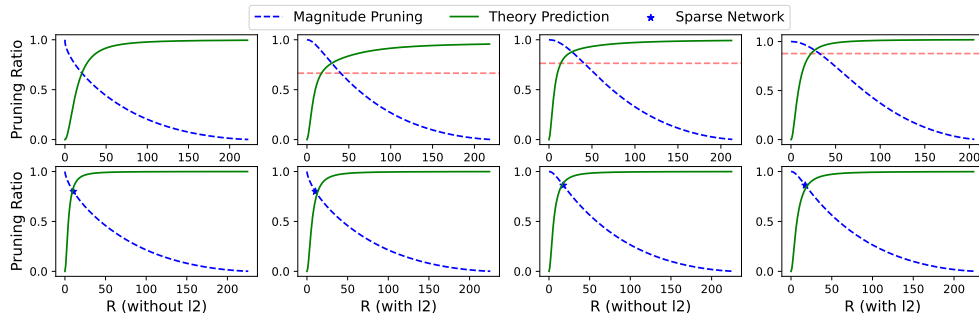


Figure 4: **Top Row:** The theoretical pruning ratio threshold in IMP of ResNet50 on Tiny-Imagenet, respectively. From left to right, as the number of iterations increases, it leads to an increase in the theoretical pruning ratio threshold. The horizontal line represents the last pruning ratio. **Bottom Row:** The comparison of the pruning ratio threshold in pruning for ResNet50 on TinyImagenet when using and not using l_2 -regularization. Sparse networks are obtained by magnitude-based pruning with fixed pruning ratios. The two plots on the left and the two plots on the right correspond to different fixed pruning ratios. Here, $R = \|\mathbf{w}^* - \mathbf{w}^k\|_2$, which is the projection distance.

7 Interpretation of Pruning Heuristics

Armed with the fundamental limit of network pruning, we’re able to provide rigorous interpretations of many heuristics employed by existing pruning algorithms.

Pruning ratio adjustment is needed in IMP. In the IMP (Iterative Magnitude Pruning) work, we determine the pruning ratio thresholds for various stages through calculations, as depicted in the top row of Figure 4. It is noteworthy that as the pruning depth gradually increases, the theoretical pruning ratio threshold also increases. Therefore, it is appropriate to prune smaller proportions of weights gradually during iterative pruning, in this context, the pruning rate refers to the proportion of retained weights in the current active weights (chosen by a mask) during this pruning operation. Both [ZG17] and [SSY⁺22] have employed pruning rate adjustment algorithms, gradually pruning smaller proportions of the weights with the iteration of the algorithm.

l_2 -regularization enhances the performance of Rare Gems. In Rare Gems, [SSY⁺22] shows that the use of l_2 regularization and its absence led to significant differences in the final performance, we have similarly scrutinized the differences between these approaches during pruning as is shown in the bottom row of Figure 4. We have discovered that when l_2 -regularization is applied, the pruning ratios tend to be larger than the theoretical limits, whereas the absence of l_2 -regularization results in excessive pruning, which can be regarded as wrong pruning.

8 Conclusion

In this paper we explore the fundamental limit of pruning ratio of deep networks by taking a first principle approach and utilizing the framework of convex geometry, thus the pruning limit problem can be reduced to determining whether two sets intersect. Through this geometric perspective, powerful tools, such as statistical dimension and approximate kinematic formula, can be leveraged. Thus we can for the first time precisely characterize the fundamental limit of network pruning ratio. The extra message conveyed by our fundamental limit is that the network pruning threshold is mostly determined by the magnitude of the weight vector as well as network flatness. Equipped with this guidelines, we're also able to provide intuitive explanations of several heuristics of existing pruning algorithms. Moreover, to address the challenges in computing the involved Gaussian width, we develop an improved spectrum estimation for large-scale and non-positive Hessian matrices. Experiments demonstrate the high accuracy of our theoretical result.

Future work. A key message from the fundamental limit of pruning ratio is that it is highly dependent on the network flatness (defined as the trace of the Hessian matrix), it is worthy trying to utilize the flatness as a regularizer when training the networks. In addition, inspired by the fact that the pruning ratio limit of a DNN is succinctly determined by the statistical dimension of a given set induced by the Hessian matrix, it's natural to ask: whether the statistical dimension can be served as a measure of the capacity of the DNN? In another regard, the pruning procedures considered in our paper is conducted after the training, an intriguing problem is: whether is it possible to prune the network before the training, and what's its fundamental limit correspondingly?

9 Impact Statements

Our work aims to advance the theoretical understanding of network pruning, with the anticipation that theoretical insights can guide future designs of network pruning methods. There are no ethically related issues or negative societal consequences in our work.

References

- [ALMT14] Dennis Amelunxen, Martin Lotz, Michael B. McCoy, and Joel A. Tropp. Living on the edge: Phase transitions in convex programs with random data, 2014.
- [BSS20] Alfonso S. Bandeira, Amit Singer, and Thomas Strohmer. *Mathematics of Data Science*. 2020.
- [CRPW12] Venkat Chandrasekaran, Benjamin Recht, Pablo A Parrilo, and Alan S Willsky. The convex geometry of linear inverse problems. *Foundations of Computational mathematics*, 12:805–849, 2012.
- [FC18] Jonathan Frankle and Michael Carbin. The lottery ticket hypothesis: Finding sparse, trainable neural networks. *arXiv preprint arXiv:1803.03635*, 2018.
- [FDRC20a] Jonathan Frankle, Gintare Karolina Dziugaite, Daniel Roy, and Michael Carbin. Linear mode connectivity and the lottery ticket hypothesis. In *International Conference on Machine Learning*, pages 3259–3269. PMLR, 2020.
- [FDRC20b] Jonathan Frankle, Gintare Karolina Dziugaite, Daniel M Roy, and Michael Carbin. Pruning neural networks at initialization: Why are we missing the mark? *arXiv preprint arXiv:2009.08576*, 2020.
- [GLC⁺23] Khashayar Gatmiry, Zhiyuan Li, Ching-Yao Chuang, Sashank Reddi, Tengyu Ma, and Stefanie Jegelka. The inductive bias of flatness regularization for deep matrix factorization. *arXiv preprint arXiv:2306.13239*, 2023.
- [GYC16] Yiwen Guo, Anbang Yao, and Yurong Chen. Dynamic network surgery for efficient dnns. *Advances in neural information processing systems*, 29, 2016.

- [HLW⁺19] Yang He, Ping Liu, Ziwei Wang, Zhilan Hu, and Yi Yang. Filter pruning via geometric median for deep convolutional neural networks acceleration. In *Proceedings of the IEEE/CVF conference on computer vision and pattern recognition*, pages 4340–4349, 2019.
- [HMD15] Song Han, Huizi Mao, and William J Dally. Deep compression: Compressing deep neural networks with pruning, trained quantization and huffman coding. *arXiv preprint arXiv:1510.00149*, 2015.
- [HPTD15] Song Han, Jeff Pool, John Tran, and William Dally. Learning both weights and connections for efficient neural network. *Advances in neural information processing systems*, 28, 2015.
- [HZRS16] Kaiming He, Xiangyu Zhang, Shaoqing Ren, and Jian Sun. Deep residual learning for image recognition. In *Proceedings of the IEEE conference on computer vision and pattern recognition*, pages 770–778, 2016.
- [KH⁺09] Alex Krizhevsky, Geoffrey Hinton, et al. Learning multiple layers of features from tiny images. 2009.
- [KSH17] Alex Krizhevsky, Ilya Sutskever, and Geoffrey E Hinton. Imagenet classification with deep convolutional neural networks. *Communications of the ACM*, 60(6):84–90, 2017.
- [LDS89] Yann LeCun, John Denker, and Sara Solla. Optimal brain damage. *Advances in neural information processing systems*, 2, 1989.
- [LFBG21] Brett W Larsen, Stanislav Fort, Nic Becker, and Surya Ganguli. How many degrees of freedom do we need to train deep networks: a loss landscape perspective. *arXiv preprint arXiv:2107.05802*, 2021.
- [LKD⁺16] Hao Li, Asim Kadav, Igor Durdanovic, Hanan Samet, and Hans Peter Graf. Pruning filters for efficient convnets. *arXiv preprint arXiv:1608.08710*, 2016.
- [Lok20] Lokesh. Tinyimagenet process in freecodecamp, 2020.
- [LY15] Ya Le and Xuan Yang. Tiny imagenet visual recognition challenge. *CS 231N*, 7(7):3, 2015.
- [LZZ⁺18] Jian-Hao Luo, Hao Zhang, Hong-Yu Zhou, Chen-Wei Xie, Jianxin Wu, and Weiyao Lin. Thinet: pruning cnn filters for a thinner net. *IEEE transactions on pattern analysis and machine intelligence*, 41(10):2525–2538, 2018.
- [MTK⁺16] Pavlo Molchanov, Stephen Tyree, Tero Karras, Timo Aila, and Jan Kautz. Pruning convolutional neural networks for resource efficient inference. *arXiv preprint arXiv:1611.06440*, 2016.
- [PCL⁺22] Mansheej Paul, Feng Chen, Brett W Larsen, Jonathan Frankle, Surya Ganguli, and Gintare Karolina Dziugaite. Unmasking the lottery ticket hypothesis: What’s encoded in a winning ticket’s mask? *arXiv preprint arXiv:2210.03044*, 2022.
- [PKA⁺21] Henning Petzka, Michael Kamp, Linara Adilova, Cristian Sminchisescu, and Mario Boley. Relative flatness and generalization. *Advances in neural information processing systems*, 34:18420–18432, 2021.
- [SCC⁺20] Jingtong Su, Yihang Chen, Tianle Cai, Tianhao Wu, Ruiqi Gao, Liwei Wang, and Jason D Lee. Sanity-checking pruning methods: Random tickets can win the jackpot. *Advances in neural information processing systems*, 33:20390–20401, 2020.
- [SSY⁺22] Kartik Sreenivasan, Jy-yong Sohn, Liu Yang, Matthew Grinde, Alliot Nagle, Hongyi Wang, Eric Xing, Kangwook Lee, and Dimitris Papailiopoulos. Rare gems: Finding lottery tickets at initialization. *Advances in Neural Information Processing Systems*, 35:14529–14540, 2022.
- [SZ14] Karen Simonyan and Andrew Zisserman. Very deep convolutional networks for large-scale image recognition. *arXiv preprint arXiv:1409.1556*, 2014.
- [Tal95] Michel Talagrand. Concentration of measure and isoperimetric inequalities in product spaces. *Publications Mathématiques de l’Institut des Hautes Etudes Scientifiques*, 81:73–205, 1995.
- [Tal96a] M. Talagrand. New concentration inequalities for product spaces. *Inventiones Math.*, 126:505–563, 1996.
- [Tal96b] M. Talagrand. A New Look at Independence. *Ann. Probab.*, 24:1–34, 1996.

- [Tao12] Terence Tao. *Topics in random matrix theory*, volume 132. American Mathematical Soc., 2012.
- [Ver14] Roman Vershynin. Estimation in high dimensions: a geometric perspective, 2014.
- [Ver20] Roman Vershynin. High-dimensional probability. *University of California, Irvine*, 2020.
- [WYD⁺18] Xin Wang, Fisher Yu, Zi-Yi Dou, Trevor Darrell, and Joseph E Gonzalez. Skipnet: Learning dynamic routing in convolutional networks. In *Proceedings of the European Conference on Computer Vision (ECCV)*, pages 409–424, 2018.
- [XWS⁺21] Qian Xiang, Xiaodan Wang, Yafei Song, Lei Lei, Rui Li, and Jie Lai. One-dimensional convolutional neural networks for high-resolution range profile recognition via adaptively feature recalibrating and automatically channel pruning. *International Journal of Intelligent Systems*, 36(1):332–361, 2021.
- [YCS17] Tien-Ju Yang, Yu-Hsin Chen, and Vivienne Sze. Designing energy-efficient convolutional neural networks using energy-aware pruning. In *Proceedings of the IEEE conference on computer vision and pattern recognition*, pages 5687–5695, 2017.
- [YGKM20] Zhewei Yao, Amir Gholami, Kurt Keutzer, and Michael W Mahoney. Pyhessian: Neural networks through the lens of the hessian. In *2020 IEEE international conference on big data (Big data)*, pages 581–590. IEEE, 2020.
- [ZAP16] Hao Zhou, Jose M Alvarez, and Fatih Porikli. Less is more: Towards compact cnns. In *Computer Vision–ECCV 2016: 14th European Conference, Amsterdam, The Netherlands, October 11–14, 2016, Proceedings, Part IV 14*, pages 662–677. Springer, 2016.
- [ZG17] Michael Zhu and Suyog Gupta. To prune, or not to prune: exploring the efficacy of pruning for model compression, 2017.

A Experimental Details

In this section, we describe the datasets, models, hyper-parameter choices and eigenspectrum adjustment used in our experiments. All of our experiments are run using PyTorch 1.12.1 on Nvidia RTX3090s with ubuntu20.04-cuda11.3.1-cudnn8 docker.

A.1 Dataset

CIFAR-10. CIFAR-10 consists of 60,000 color images, with each image belonging to one of ten different classes with size 32×32 . The classes include common objects such as airplanes, automobiles, birds, cats, deer, dogs, frogs, horses, ships, and trucks. The CIFAR-10 dataset is divided into two subsets: a training set and a test set. The training set contains 50,000 images, while the test set contains 10,000 images [KH⁺09]. For data processing, we follow the standard augmentation: normalize channel-wise, randomly horizontally flip, and random cropping.

CIFAR-100. The CIFAR-100 dataset consists of 60,000 color images, with each image belonging to one of 100 different fine-grained classes [KH⁺09]. These classes are organized into 20 superclasses, each containing 5 fine-grained classes. Similar to CIFAR-10, the CIFAR-100 dataset is split into a training set and a test set. The training set contains 50,000 images, and the test set contains 10,000 images. Each image is of size 32×32 pixels and is labeled with its corresponding fine-grained class. Augmentation includes normalize channel-wise, randomly horizontally flip, and random cropping.

TinyImageNet. TinyImageNet comprises 100,000 images distributed across 200 classes, with each class consisting of 500 images [LY15]. These images have been resized to 64×64 pixels and are in full color. Each class encompasses 500 training images, 50 validation images, and 50 test images. Data augmentation techniques encompass normalization, random rotation, and random flipping. The dataset includes distinct train, validation, and test sets for experimentation. For data preprocessing, please refer to [Lok20].

A.2 Model

In all experiments, pruning skips bias and batchnorm, which have little effect on the sparsity of the network. Use non-affine batchnorm in the network, and the initialization of the network is kaiming normal initialization.

Full Connect Network(FC-5, FC-12). We train a five-layer fully connected network (FC-5) and a twelve-layer fully connected network FC-12 on CIFAR-10, the network architecture details can be found in Table 4.

Table 4: FC-5 and FC-12 architecture used in our experiments.

Model	Layer Width
FC-5	1000, 600, 300, 100, 10
FC-12	1000, 900, 800, 750, 700, 650, 600, 500, 400, 200, 100, 10

AlexNet [KSH17]. We use the standard AlexNet architecture. In order to use CIFAR-10 to train AlexNet, we upsample each picture of CIFAR-10 to $3 \times 224 \times 224$. The detailed network architecture parameters are shown in Table 5.

VGG-16 [SZ14]. In the original VGG-16 network, there are 13 convolution layers and 3 FC layers (including the last linear classification layer). We follow the VGG-16 architectures used in [FDRC20a, FDRC20b] to remove the first two FC layers while keeping the last linear classification layer. This finally leads to a 14-layer architecture, but we still call it VGG-16 as it is modified from the original VGG-16 architectural design. Detailed architecture is shown in Table 6. VGG-16 is trained on CIFAR-10.

Table 5: AlexNet architecture used in our experiments.

Layer	Shape	Stride	Padding
conv1	$3 \times 96 \times 11 \times 11$	4	1
max pooling	kernel size:3	2	N/A
conv2	$96 \times 256 \times 5 \times 5$	1	2
max pooling	kernel size:3	2	N/A
conv3	$256 \times 384 \times 3 \times 3$	1	1
conv4	$384 \times 384 \times 3 \times 3$	1	1
conv4	$384 \times 256 \times 3 \times 3$	1	1
max pooling	kernel size:3	2	N/A
linear1	6400×4096	N/A	N/A
linear1	4096×4096	N/A	N/A
linear1	4096×10	N/A	N/A

Table 6: VGG-16 architecture used in our experiments.

Layer	Shape	Stride	Padding
conv1	$3 \times 64 \times 3 \times 3$	1	1
conv2	$64 \times 64 \times 3 \times 3$	1	1
max pooling	kernel size:2	2	N/A
conv3	$64 \times 128 \times 3 \times 3$	1	1
conv4	$128 \times 128 \times 3 \times 3$	1	1
max pooling	kernel size:2	2	N/A
conv5	$128 \times 256 \times 3 \times 3$	1	1
conv6	$256 \times 256 \times 3 \times 3$	1	1
conv7	$256 \times 256 \times 3 \times 3$	1	1
max pooling	kernel size:2	2	N/A
conv8	$256 \times 512 \times 3 \times 3$	1	1
conv9	$512 \times 512 \times 3 \times 3$	1	1
conv10	$512 \times 512 \times 3 \times 3$	1	1
max pooling	kernel size:2	2	N/A
conv11	$512 \times 512 \times 3 \times 3$	1	1
conv12	$512 \times 512 \times 3 \times 3$	1	1
conv13	$512 \times 512 \times 3 \times 3$	1	1
max pooling	kernel size:2	2	N/A
avg pooling	kernel size:1	1	N/A
linear1	512×10	N/A	N/A

Table 7: ResNet architecture used in our experiments.

Layer	ResNet-18	ResNet-50
conv1	$64, 3 \times 3; \text{stride:1; padding:1}$	$64, 3 \times 3; \text{stride:1; padding:1}$
block1	$\begin{pmatrix} 64, 3 \times 3; \text{stride:1; padding:1} \\ 64, 3 \times 3; \text{stride:1; padding:1} \end{pmatrix} \times 2$	$\begin{pmatrix} 64, 1 \times 1; \text{stride:1; padding:0} \\ 64, 3 \times 3; \text{stride:1; padding:1} \\ 256, 1 \times 1; \text{stride:1; padding:0} \end{pmatrix} \times 3$
block1	$\begin{pmatrix} 128, 3 \times 3; \text{stride:2; padding:1} \\ 128, 3 \times 3; \text{stride:1; padding:1} \end{pmatrix} \times 2$	$\begin{pmatrix} 128, 1 \times 1; \text{stride:1; padding:0} \\ 128, 3 \times 3; \text{stride:2; padding:1} \\ 512, 3 \times 3; \text{stride:1; padding:0} \end{pmatrix} \times 4$
block1	$\begin{pmatrix} 128, 3 \times 3; \text{stride:2; padding:1} \\ 256, 3 \times 3; \text{stride:1; padding:1} \end{pmatrix} \times 2$	$\begin{pmatrix} 256, 1 \times 1; \text{stride:1; padding:0} \\ 256, 3 \times 3; \text{stride:2; padding:1} \\ 1024, 1 \times 1; \text{stride:1; padding:0} \end{pmatrix} \times 6$
block1	$\begin{pmatrix} 512, 3 \times 3; \text{stride:2; padding:1} \\ 512, 3 \times 3; \text{stride:1; padding:0} \end{pmatrix} \times 2$	$\begin{pmatrix} 512, 1 \times 1; \text{stride:1; padding:1} \\ 512, 3 \times 3; \text{stride:2; padding:1} \\ 2048, 1 \times 1; \text{stride:1; padding:0} \end{pmatrix} \times 3$
avg pooling	kernel size:1; stride:1	kernel size:1; stride:1
linear1	$512 \times \text{ClassNum}$	$2048 \times \text{ClassNum}$

ResNet-18 and ResNet-50 [HZRS16]. We use the standard ResNet architecture for TinyImageNet and tune it for the CIFAR-100 dataset. The detailed network architecture parameters are shown in Table 7. ResNet-18 and ResNet-50 is trained on CIFAR-100 and TinyImageNet.

A.3 Training Hyper-parameters Setup

In this section, we will describe in detail the training hyper-parameters of the Global One-shot Pruning algorithm on multiple datasets and models. The various hyperparameters are detailed in Table 8.

Table 8: Hyper Parameters used for different Datasets and Models.

Model	Dataset	Batch Size	Epochs	Optimizer	LR	Momentum	Warm Up	Weight Decay	CosineLR	Lambda
FC5	CIFAR10	128	200	SGD	0.01	0.9	0	0	N/A	0.00005
FC12	CIFAR10	128	200	SGD	0.01	0.9	0	0	N/A	0.00005
VGG16	CIFAR10	128	200	SGD	0.01	0.9	5	0	True	0.00015
AlexNet	CIFAR10	128	200	SGD	0.01	0.9	5	0	True	0.00003
ResNet18	CIFAR100	128	200	SGD	0.1	0.9	5	0	True	0.000055
ResNet50	CIFAR100	128	200	SGD	0.1	0.9	5	0	True	0.00002
ResNet18	TinyImageNet	128	200	SGD	0.01	0.9	5	0	True	0.00023
ResNet50	TinyImageNet	128	200	SGD	0.01	0.9	5	0	True	0.0001

A.4 Sublevel Set Parameters Setup.

Given that the test data is often unavailable and the network can ensure the Hessian matrix is positive definite as much as possible by utilizing the training data for computation. Additionally, we generally assume that the training and test data share the same distribution, thus we use the training data to define the loss sublevel set as $\hat{\epsilon} = \epsilon - \mathcal{L}(\mathbf{w}_0)$. We compute the standard deviation of the network’s loss across multiple batches on the training data set and denote it by $\hat{\epsilon}$.

A.5 Loss Sub-level Set

Given a dense well-trained neural network M with weighted donated as \mathbf{w}^* , the loss sublevel set is $\{\mathbf{w} \in \mathbb{R}^D : \frac{1}{2} \hat{\mathbf{w}}^T \mathbf{H} \hat{\mathbf{w}} \leq \hat{\epsilon}\}$ where $\hat{\epsilon} = \epsilon - \mathcal{L}(\mathbf{w}^*)$, as we operate under the assumption of having access only to training data, we calculate the training loss for each batch and utilize the standard deviation of all training losses as the variable $\hat{\epsilon}$.

Table 9: Hyper Parameters used in SLQ Algorithm.

Model	Dataset	Runs	Iterations	Bins	Squared Sigma
FC5	CIFAR10	1	128	100000	1e-10
FC12	CIFAR10	1	128	100000	1e-10
VGG16	CIFAR10	1	128	100000	1e-07
AlexNet	CIFAR10	1	96	100000	1e-07
ResNet18	CIFAR100	1	128	100000	1e-07
ResNet50	CIFAR100	1	128	100000	1e-07
ResNet18	TinyImageNet	1	128	100000	1e-07
ResNet50	TinyImageNet	1	88	100000	1e-07

A.6 Theoretical Pruning Ratio

Taking \mathbf{w}^* as the initial pruning point and calculating the corresponding value of R for different pruning ratios. We then plot the corresponding curve of the theoretically predicted pruning ratio and the calculated R in the same graph. The intersection point of these two curves is taken as the upper bound of the theoretically predicted pruning ratio. All results are shown in Figure 5.

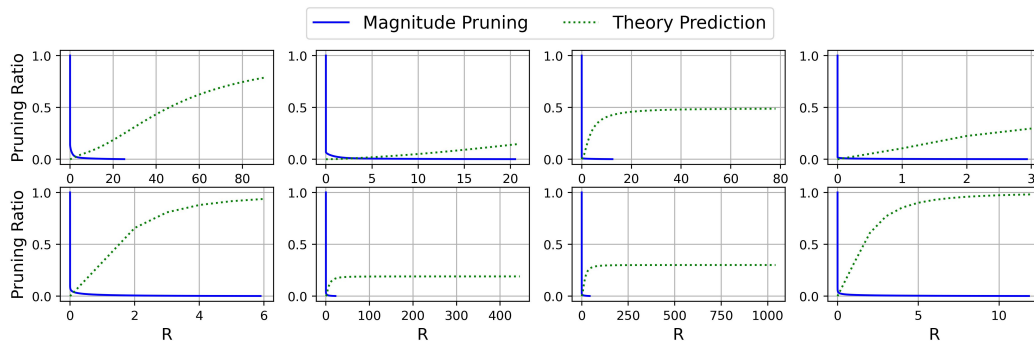


Figure 5: The theoretically predicted pruning ratio in eight tasks. The first row, from left to right, corresponds to FC5, FC12, AlexNet, and VGG16. The second row, from left to right, corresponds to ResNet18 and ResNet50 on CIFAR100, as well as ResNet18 and ResNet50 on TinyImagenet.

B Calculation of Gaussian Width

In practical experiments, determining the Gaussian width of the ellipsoid defined by the network loss function is a challenging task. There are two primary challenges encountered in this section: 1. the computation of eigenvalues for high-dimensional matrices poses significant difficulty; 2. the network fails to converge perfectly to the extremum, leading to a non-positive definite Hessian matrix for the loss function. In this section, we tackle these challenges through the utilization of a fast eigenspectrum estimation algorithm and an algorithm that approximates the Gaussian width of a deformed ellipsoid body. These approaches effectively address the aforementioned problems.

B.1 Improved SLQ (Stochastic Lanczos Quadrature) Spectrum Estimation

Calculating the eigenvalues of large matrices has long been a challenging problem in numerical analysis. One widely used method for efficiently computing these eigenvalues is the Lanczos algorithm, which is presented in Appendix B. However, due to the huge amount of parameters of the deep neural network, it is

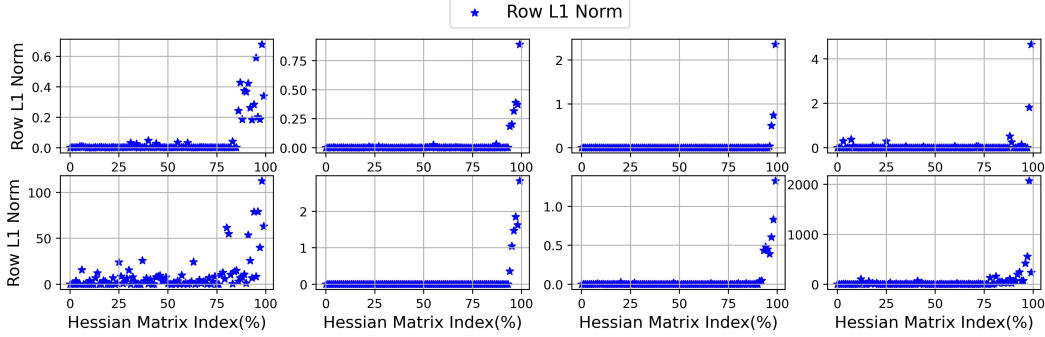


Figure 6: The statistical analysis of the L1 norm of the Hessian matrix in eight tasks. The first row, from left to right, corresponds to FC5, FC12, AlexNet, and VGG16. The second row, from left to right, corresponds to ResNet18 and ResNet50 on CIFAR100, as well as ResNet18 and ResNet50 on TinyImagenet.

still impractical to use this method to calculate the eigenspectrum of the Hessian matrix of a deep neural network. To tackle this problem, [YGKM20] proposed SLQ(Stochastic Lanczos Quadrature) Spectrum Estimation Algorithm, which estimates the overall eigenspectrum distribution based on a small number of eigenvalues obtained by Lanczos algorithm. This method enables the efficient computation of the full eigenvalues of large matrices. Algorithm 1 outlines the step-by-step procedure for the classic Lanczos algorithm, providing a comprehensive guide for its implementation. The algorithm requires the selection of the number of iterations, denoted as m , which determines the size of the resulting triangular matrix \mathbf{T} .

Algorithm 1: The Lanczos Algorithm

Input: a Hermitian matrix \mathbf{A} of size $n \times n$, a number of iterations m

Output: a tridiagonal real symmetric matrix \mathbf{T} of size $m \times m$

initialization:

1. Draw a random vector \mathbf{v}_1 of size $n \times 1$ from $\mathcal{N}(0,1)$ and normalize it;
2. $\mathbf{w}'_1 = \mathbf{A}\mathbf{v}_1$; $\alpha_1 = \langle \mathbf{w}'_1, \mathbf{v}_1 \rangle$; $\mathbf{w}_1 = \mathbf{w}'_1 - \alpha_1\mathbf{v}_1$;
- 3.

for $j = 2, \dots, m$ **do**

1). $\beta_j = \|\mathbf{w}_{j-1}\|$;

2).

if $\beta_j = 0$ **then**

stop

else

$\mathbf{v}_j = \mathbf{w}_{j-1}/\beta_j$

3). $\mathbf{w}'_j = \mathbf{A}\mathbf{v}_j$;

4). $\alpha_j = \langle \mathbf{w}'_j, \mathbf{v}_j \rangle$;

5). $\mathbf{w}_j = \mathbf{w}'_j - \alpha_j\mathbf{v}_j - \beta_j\mathbf{v}_{j-1}$;

4. $\mathbf{T}(i, i) = \alpha_i, i = 1, \dots, m$;

$\mathbf{T}(i, i + 1) = \mathbf{T}(i + 1, i) = \beta_i, i = 1, \dots, m - 1$.

Return: \mathbf{T}

In general, the Lanczos algorithm is not capable of accurately computing zero eigenvalues, and this limitation becomes more pronounced when the SLQ algorithm has a small number of iterations. Similarly, vanishingly small eigenvalues are also ignored by Lanczos. However, in a well-trained large-scale deep neural network, the experiment found that the network loss function hessian matrix has a large number of zero eigenvalues and vanishingly small eigenvalues. In the Gaussian width of the ellipsoid, the zero eigenvalues and vanishingly small eigenvalues have the same effect on the width (insensitive to other parameters), and we collectively refer to these eigenvalues as the “important” eigenvalues. We divide

the weight into 100 parts from small to large, calculate the second-order derivative (including partial derivative) of smallest weight in each part, and sum the absolute values of all second-order derivatives of the weight, which corresponds to l_1 -norm of a row in hessian matrix, and the row l_1 -norm is zero or a vanishingly small corresponds to an “important” eigenvalue, the experimental results can be seen in the first column of Figure 6, from which the number of missing eigenvalues of the SLQ algorithm can be estimated, we then add the same number of $1e-30$ as the missing eigenvalues in the Hessian matrix eigenspectrum. SLQ algorithm parameters adjustment is described in Table 9 and the statistical analysis of the l_1 norm of Hessian matrix rows for all experiments is presented in Figure 6. For details of the SLQ algorithm, see Algorithm 2

Algorithm 2: SLQ(Stochastic Lanczos Quadrature) Spectrum Estimation Algorithm

Input: A hermitian matrix \mathbf{A} of size $n \times n$, Lanczos iterations m , ESD computation iterations l , gaussian kernel f and variance σ^2 .

Output: The spectral distribution of matrix \mathbf{A}

for $i = 2, \dots, l$ **do**

1). Get the tridiagonal matrix \mathbf{T} if size $m \times m$ through Lanczos algorithm;

2). Compute $\tau_k^{(i)}$ and $\lambda_k^{(i)}$ from \mathbf{T} ;

3). $\phi_\sigma^i(t) = \sum_{k=1}^m \tau_k^{(i)} f(\lambda_k^{(i)}; t, \sigma)$;

4). $\phi(t) = \frac{1}{l} \sum_{i=1}^l \phi_\sigma^i(t)$

Return: $\phi(t)$

B.2 Gaussian Width of the Deformed Ellipsoid

After effective training, it is generally assumed that a deep neural network will converge to the global minimum of its loss function. However, in practice, even after meticulous tuning, the network tends to oscillate around the minimum instead of converging to it. This leads to that the Hessian matrix of the loss function would be non-positive definite, and the resulting geometric body defined by this matrix would change from an expected ellipsoid to a hyperboloid, which is unfortunately nonconvex. To quantify the Gaussian width of the ellipsoid corresponding to the perfect minima, we propose to approximate it by convexifying the deformed ellipsoid through replacing the associated negative eigenvalues with its absolute value. This processing turns out to be very effective, as demonstrated by the experimental results.

Lemma B.1. *Consider a well-trained neural network M with weights \mathbf{w} , whose loss function defined by \mathbf{w} has a Hessian matrix \mathbf{H} . Due to the non-positive definiteness of \mathbf{H} , there exist negative eigenvalues. Let the eigenvalue decomposition of \mathbf{H} be $\mathbf{H} = \mathbf{v}^T \mathbf{\Sigma} \mathbf{v}$, where $\mathbf{\Sigma}$ is a diagonal matrix of eigenvalues. Let $\mathbf{D} = \mathbf{v}^T |\mathbf{\Sigma}| \mathbf{v}$, where $|\cdot|$ means absolute operation. the geometric objects defined by H and D are $S(\epsilon) := \{\mathbf{w} \in \mathbb{R}^D : \frac{1}{2} \mathbf{w}^T \mathbf{H} \mathbf{w} \leq \epsilon\}$ and $\hat{S}(\epsilon) := \{\mathbf{w} \in \mathbb{R}^D : \frac{1}{2} \mathbf{w}^T \mathbf{D} \mathbf{w} \leq \epsilon\}$, then:*

$$w(S(\epsilon)) \approx w(\hat{S}(\epsilon)) \tag{B.1}$$

The proof of Lemma B.1 is in Appendix C.2. Lemma B.1 indicates that if the deep neural network converges to a vicinity of the global minimum of the loss function, the Gaussian width of the deformed ellipsoid body can be approximated by taking the convex hull of $S(\epsilon)$. Experimental results demonstrate that the two approximation methods, namely setting negative features to zero and taking absolute values, yield nearly indistinguishable outcomes.

C Theoretical Part Supplement

In this section, we provide details regarding the threshold of network pruning ratio, specifically, the dimension of the sublevel sets of quadratic wells.

C.1 Gaussian Width of the Quadratic Well

Gaussian width is an extremely useful tool to measure the complexity of a convex body. In our proof, we will use the following expression for its definition:

$$w(S) = \frac{1}{2} \mathbb{E} \sup_{\mathbf{x}, \mathbf{y} \in S} \langle \mathbf{g}, \mathbf{x} - \mathbf{y} \rangle, \mathbf{g} \sim \mathcal{N}(\mathbf{0}, \mathbf{I}_{D \times D})$$

Concentration of measure is a universal phenomenon in high-dimensional probability. Basically, it says that a random variable which depends in a smooth way on many independent random variables (but not too much on any of them) is essentially *constant*. [Tal96a, Tal96b, Tal95]

Theorem 5. (*Gaussian concentration*) Consider a random vector $\mathbf{x} \sim \mathcal{N}(\mathbf{0}, \mathbf{I}_n)$ and an L -Lipschitz function $f : \mathbb{R}^n \rightarrow \mathbb{R}$ (with respect to the Euclidean metric). Then for $t \geq 0$

$$\mathbb{P}(|f(\mathbf{x}) - \mathbb{E}f(\mathbf{x})| \geq t) \leq \epsilon, \quad \epsilon = e^{-\frac{t^2}{2L^2}}.$$

Therefore, if ϵ is small, $f(\mathbf{x})$ can be approximated as $f(\mathbf{x}) \approx \mathbb{E}f(\mathbf{x}) + \sqrt{-2L^2 \ln \epsilon}$.

Lemma C.1. Given a random vector $\mathbf{x} \sim \mathcal{N}(\mathbf{0}, \mathbf{I}_n)$ and the inverse of a positive definite Hessian matrix $\mathbf{Q} = \mathbf{H}^{-1}$, where $\mathbf{H} \in \mathbb{R}^{n \times n}$, we have:

$$\mathbb{E} \sqrt{\mathbf{x}^T \mathbf{Q} \mathbf{x}} \approx \sqrt{\mathbb{E} \mathbf{x}^T \mathbf{Q} \mathbf{x}}$$

Proof.

- 1.) Concentration of $\mathbf{x}^T \mathbf{Q} \mathbf{x}$
Define $f(\mathbf{x}) = \mathbf{x}^T \mathbf{Q} \mathbf{x}$, we have

$$\begin{aligned} f(\mathbf{x}) &= \mathbf{x}^T \mathbf{Q} \mathbf{x} \\ &= \mathbf{x}^T \mathbf{U} \Sigma \mathbf{U}^T \mathbf{x} && \text{Eigenvalue Decomposition of } \mathbf{Q} : \mathbf{Q} = \mathbf{U} \Sigma \mathbf{U}^T. \\ &= \sum_{i=1}^n \lambda_i x_i^2 && \text{Invariance of Gaussian under rotation.} \end{aligned}$$

where λ_i is the eigenvalue of \mathbf{Q} . The lipschitz constant L_f of function $f(\mathbf{x})$ is :

$$L_f = \max\left(\left|\frac{\partial f}{\partial \mathbf{x}}\right|\right) = \max(|2\lambda_i x_i|)$$

Let $g(x_i) = 2\lambda_i x_i$, whose lipschitz constant is $L_g = |2\lambda_i|$. Invoking Theorem 5, we have:

$$\begin{aligned} g(x_i) &\approx \mathbb{E}g(x_i) + \sqrt{-2(2\lambda_i)^2 \ln \epsilon_1} \\ &= \sqrt{-8\lambda_i^2 \ln \epsilon_1}. \end{aligned}$$

Therefore, the lipschitz constant of $f(\mathbf{x})$ can be approximated by:

$$L_f = \max(\sqrt{-8\lambda_i^2 \ln \epsilon_1}) = \sqrt{-8 \ln \epsilon_1} \lambda_{max}$$

Invoking Theorem 5 again, we establish the concentration of $f(\mathbf{x})$ as follows:

$$\begin{aligned} f(\mathbf{x}) &\approx \mathbb{E}f(\mathbf{x}) + \sqrt{-2(L_f)^2 \ln \epsilon_2} && \text{Theorem 5.} \\ &= \mathbb{E}f(\mathbf{x}) + 4\sqrt{\ln \epsilon_1 \ln \epsilon_2} \lambda_{max} \end{aligned}$$

- 2.) Jensen ratio of $\sqrt{\mathbf{x}^T \mathbf{Q} \mathbf{x}}$:

$$\begin{aligned} \mathbb{E} \sqrt{f(\mathbf{x})} &\approx \mathbb{E} \sqrt{\mathbb{E}f(\mathbf{x}) + 4\sqrt{\ln \epsilon_1 \ln \epsilon_2} \lambda_{max}} && \text{Concentration of } f(\mathbf{x}). \\ &\approx \sqrt{\mathbb{E}f(\mathbf{x})} + \frac{2\sqrt{\ln \epsilon_1 \ln \epsilon_2} \lambda_{max}}{\sqrt{\mathbb{E}f(\mathbf{x})}} && \text{Taylor Expansion.} \end{aligned}$$

Therefore, the Jensen ratio of $\sqrt{f(\mathbf{x})}$ equals:

$$\begin{aligned}\frac{\mathbb{E}\sqrt{f(\mathbf{x})}}{\sqrt{\mathbb{E}f(\mathbf{x})}} &= 1 + 2\sqrt{\ln\epsilon_1\ln\epsilon_2} \frac{\lambda_{max}}{\sum_{i=1}^n \lambda_i} \\ &= 1 + \delta\end{aligned}$$

If \mathbf{Q} is a Wishart matrix, i.e. $\mathbf{Q} = \mathbf{A}^T \mathbf{A}$, where \mathbf{A} is a random matrix whose elements are independently and identically distributed with unit variance, according to the Marchenko-Pastur law [Tao12], the maximum eigenvalue of \mathbf{Q} is approximately $4n$ and the trace of \mathbf{Q} is approximately n^2 . Therefore, the above Jensen ratio approaches to 1 with decaying rate $\mathcal{O}(\frac{1}{n})$.

For the inverse of a positive definite Hessian matrix which is of our concern, we take $\epsilon_1 = \epsilon_2 = 10^{-4}$, numerical simulations show that when the dimension $n = 10^5$, the corresponding δ in the above Jensen ratio is on the order of 10^{-3} , which is in good agreement with the theoretical value and is arguably negligible. Similar as the case of the above-discussed Wishart matrix, when the dimension n increases, the value of δ will further decrease.

Definition C.2. (Definition of ball) A (closed) ball $B(c, r)$ (in \mathbb{R}^D) centered at $c \in \mathbb{R}^D$ with radius r is the set

$$B(c, r) := \{\mathbf{x} \in \mathbb{R}^D : \mathbf{x}^T \mathbf{x} \leq r^2\}$$

The set $B(0, 1)$ is called the unit ball. An ellipsoid is just an affine transformation of a ball.

Lemma C.3. (Definition of ellipsoid). An ellipsoid S centered at the origin is the image $L(B(0, 1))$ of the unit ball under an invertible linear transformation $L : \mathbb{R}^D \rightarrow \mathbb{R}^D$. An ellipsoid centered at a general point $c \in \mathbb{R}^D$ is just the translate $c + S$ of some ellipsoid S centered at the origin.

Proof.

$$\begin{aligned}L(B(0, 1)) &= \{\mathbf{L}\mathbf{x} : \mathbf{x} \in B(0, 1)\} \\ &= \{\mathbf{y} : \mathbf{L}^{-1}\mathbf{y} \in B(0, 1)\} \\ &= \{\mathbf{y} : (\mathbf{L}^{-1}\mathbf{y})^T \mathbf{L}^{-1}\mathbf{y} \leq 1\} \\ &= \{\mathbf{y} : \mathbf{y}^T (\mathbf{L}\mathbf{L}^T)^{-1} \mathbf{y} \leq 1\} \\ &= \{\mathbf{y} : \mathbf{y}^T \mathbf{Q}^{-1} \mathbf{y} \leq 1\}\end{aligned}$$

where $\mathbf{Q} = \mathbf{L}\mathbf{L}^T$ is **positive definite**.

The radius r_i along principal axis \mathbf{e}_i obeys $r_i^2 = \frac{1}{\lambda_i}$, where λ_i is the eigenvalue of \mathbf{Q}^{-1} and \mathbf{e}_i is eigen vector.

Lemma C.4. (Gaussian width of ellipsoid). Let S be an ellipsoid in \mathbb{R}^D defined by the positive definite matrix $\mathbf{H} \in \mathbb{R}^{D \times D}$:

$$S(\epsilon) := \{\mathbf{w} \in \mathbb{R}^D : \frac{1}{2} \mathbf{w}^T \mathbf{H} \mathbf{w} \leq \epsilon\}$$

Then $w(S)^2$ or the Gaussian width squared of the ellipsoid satisfies:

$$w(S)^2 \approx 2\epsilon \text{Tr}(\mathbf{H}^{-1}) = \sum_i r_i^2$$

where $r_i = \sqrt{2\epsilon/\lambda_i}$ with λ_i is i -th eigenvalue of \mathbf{H} .

Proof. Let $\mathbf{g} \sim \mathcal{N}(\mathbf{0}, \mathbf{I}_{D \times D})$ and $\mathbf{L}\mathbf{L}^T = 2\epsilon\mathbf{H}^{-1}$. Then:

$$\begin{aligned}
w(L(B_2^n)) &= \frac{1}{2} \mathbb{E} \sup_{\mathbf{x}, \mathbf{y} \in B(0,1)} \langle \mathbf{g}, \mathbf{L}\mathbf{x} - \mathbf{L}\mathbf{y} \rangle \\
&= \frac{1}{2} \mathbb{E} \sup_{\mathbf{x}, \mathbf{y} \in B(0,1)} \langle \mathbf{g}\mathbf{L}, \mathbf{x} - \mathbf{y} \rangle \\
&= \mathbb{E} \|\mathbf{g}\mathbf{L}\|_2 && \text{Definition of Ball.} \\
&= \mathbb{E} \sqrt{(\mathbf{g}\mathbf{L}\mathbf{L}^T\mathbf{g}^T)} && \|\mathbf{g}\|_2 = \sqrt{\mathbf{g}\mathbf{g}^T}, \text{ where } \mathbf{g} \in \mathbb{R}^{1 \times D}. \\
&= \mathbb{E} \sqrt{2\epsilon\mathbf{g}\mathbf{H}^{-1}\mathbf{g}^T} \\
&\approx \sqrt{2\epsilon\mathbb{E}[\mathbf{g}\mathbf{H}^{-1}\mathbf{g}^T]} && \text{Lemma C.1.} \\
&= \sqrt{2\epsilon\text{Tr}(\mathbf{H}^{-1})} && \text{Invariance of Gaussian under rotation.}
\end{aligned}$$

Thus, $w(S)^2 \approx 2\epsilon\text{Tr}(\mathbf{H}^{-1}) = \sum_i^D r_i^2$.

C.2 Gaussian Width of the Deformed Ellipsoid

Generally, it is assumed that the gradient descent algorithm will converge to a minimum point. However, in practice, even with small learning rates, the network may oscillate near the minimum point and not directly converge to it, but rather get very close to it. As a result, the actual Hessian matrix is often not positive definite and its eigenvalues may have negative values.

Lemma C.5. *Let the Hessian matrix at the minimum point be denoted by \mathbf{H} with eigenvalue λ_i , and the Hessian matrix at an oscillation point be denoted by $\hat{\mathbf{H}}$ with eigenvalue $\hat{\lambda}_i$. The negative eigenvalues of $\hat{\mathbf{H}}$ have small magnitudes.*

Proof. Let the weights at the minimum point be denoted by \mathbf{w}_0 and the Hessian matrix at an oscillation point be denoted by $\hat{\mathbf{w}}_0$. Consider a loss function L and a loss landscape defined by $L(\mathbf{w})$, taking Taylor expansion of $L(\mathbf{w})$ at \mathbf{w}_0 :

$$L(\mathbf{w}) = L(\mathbf{w}_0) + \frac{1}{2}(\mathbf{w} - \mathbf{w}_0)^T \mathbf{H}(\mathbf{w} - \mathbf{w}_0) + R(\mathbf{w}_0)$$

Let $\hat{\mathbf{w}}_0 = \mathbf{w}_0 + \mathbf{v}$ with \mathbf{v} is closed to $\mathbf{0}$:

$$\begin{aligned}
L(\hat{\mathbf{w}}_0) &= L(\mathbf{w}_0 + \mathbf{v}) \\
&= L(\mathbf{w}_0) + \frac{1}{2}\mathbf{v}^T \mathbf{H}\mathbf{v} + R(\mathbf{w}_0 + \mathbf{v})
\end{aligned}$$

Therefore, the second order derivative of $L(\hat{\mathbf{w}}_0)$ is:

$$\begin{aligned}
L''(\mathbf{w}) &= L''(\mathbf{w}_0 + \mathbf{v}) \\
&= \mathbf{H} + R''(\mathbf{w}_0 + \mathbf{v}) \\
&\approx \mathbf{H}
\end{aligned}$$

where $L''(\mathbf{w}) = \hat{\mathbf{H}}$, Let $\mathbf{H} = \hat{\mathbf{H}} + \mathbf{H}_0$ with \mathbf{H}_0 is closed to $\mathbf{0}$, considering the Weyl inequality:

$$\lambda_i(\mathbf{H}) - \hat{\lambda}_i(\hat{\mathbf{H}}) \leq \|\mathbf{H}_0\|_2$$

where $\|\mathbf{H}_0\|_2$ is small enough. So if $\hat{\lambda}_i(\hat{\mathbf{H}})$ is less than 0, since $\hat{\lambda}_i(\hat{\mathbf{H}}) \geq \lambda_i(\mathbf{H}) - \|\mathbf{H}_0\|_2$, its absolute value $|\hat{\lambda}_i(\hat{\mathbf{H}})| \leq \|\mathbf{H}_0\|_2 - \lambda_i(\mathbf{H}) \leq \|\mathbf{H}_0\|_2$, which means that the negative eigenvalues of the Hessian matrix have small magnitudes.

Lemma C.6. *For a sublevel set $S(\epsilon) := \{\mathbf{w} : \mathbf{w}^T \mathbf{H} \mathbf{w} \leq \epsilon\}$ defined by a matrix \mathbf{H} with small magnitude negative eigenvalues. The Gaussian width of $S(\epsilon)$ can be estimated by obtaining the absolute values of the eigenvalues of the matrix \mathbf{H} .*

Proof. Assuming that the eigenvalue decomposition of \mathbf{H} is $\mathbf{H} = \mathbf{v}^T \boldsymbol{\Sigma} \mathbf{v}$, where $\boldsymbol{\Sigma}$ is a diagonal matrix consisting of the eigenvalues of \mathbf{H} , let $\mathbf{D} = \mathbf{v}^T |\boldsymbol{\Sigma}| \mathbf{v}$ be a positive definite matrix and $\mathbf{M} = \mathbf{H} - \mathbf{D} = \mathbf{v}^T (\boldsymbol{\Sigma} - |\boldsymbol{\Sigma}|) \mathbf{v}$ be a negative definite matrix. Consider the definition of $S(\epsilon)$:

$$\begin{aligned} \mathbf{w}^T \mathbf{H} \mathbf{w} &= \mathbf{w}^T (\mathbf{H} - \mathbf{D} + \mathbf{D}) \mathbf{w} \\ &= \mathbf{w}^T \mathbf{M} \mathbf{w} + \mathbf{w}^T \mathbf{D} \mathbf{w} \\ &\leq \epsilon \end{aligned}$$

Therefore, $S(\epsilon)$ can be expressed as $\mathbf{w}^T \mathbf{D} \mathbf{w} \leq \epsilon - \mathbf{w}^T \mathbf{M} \mathbf{w}$. Since the magnitudes of the negative eigenvalues of \mathbf{H} are very small, we can assume that $\mathbf{w}^T \mathbf{M} \mathbf{w}$ is also small, and thus $\mathbf{w}^T \mathbf{D} \mathbf{w} \leq \epsilon - \mathbf{w}^T \mathbf{M} \mathbf{w}$ can be approximately equal to $\mathbf{w}^T \mathbf{D} \mathbf{w} \leq \epsilon$. As a result, we can estimate the Gaussian width of $S(\epsilon)$ by approximating it with the absolute values of the eigenvalues of \mathbf{H} .

Corollary C.7. *Consider a well-trained neural network M with weights \mathbf{w} , whose loss function defined by \mathbf{w} has a Hessian matrix \mathbf{H} . Due to the non-positive definiteness of \mathbf{H} , there exist negative eigenvalues. Let the eigenvalue decomposition of \mathbf{H} be $\mathbf{H} = \mathbf{v}^T \boldsymbol{\Sigma} \mathbf{v}$, where $\boldsymbol{\Sigma}$ is a diagonal matrix of eigenvalues. Let $\mathbf{D} = \mathbf{v}^T |\boldsymbol{\Sigma}| \mathbf{v}$, where $|\cdot|$ means absolute operation. The geometric objects defined by H and D are $S(\epsilon) := \{\mathbf{w} \in \mathbb{R}^D : \frac{1}{2} \mathbf{w}^T \mathbf{H} \mathbf{w} \leq \epsilon\}$ and $\hat{S}(\epsilon) := \{\mathbf{w} \in \mathbb{R}^D : \frac{1}{2} \mathbf{w}^T \mathbf{D} \mathbf{w} \leq \epsilon\}$, then:*

$$w(S(\epsilon)) \approx w(\hat{S}(\epsilon))$$

D Comparison between the Upper and Lower Bound

This section provided the proofs of the lower bound derivation and roughly analyzed how the lower bound changes when the upper bound varies.

D.1 $D - m$ Dimension Sublevel Set is Still an Ellipsoid

In the derivation of the lower bound for the pruning ratio threshold, we employed a $D - m$ dimensional loss sublevel set:

$$S(\mathbf{w}^2) = \{\mathbf{w}^2 \in \mathbb{R}^{D-m} : \mathcal{L}(\mathbf{w}^1, \mathbf{w}^2) \leq \epsilon\} \quad (\text{D.1})$$

Perform Taylor expansion to $\mathcal{L}(\mathbf{w}^1, \mathbf{w}^2)$ with respect to \mathbf{w}^2 , the sublevel set is represented as:

$$S(\mathbf{w}^2) = \{\mathbf{w}^2 \in \mathbb{R}^{D-m} : \frac{1}{2} (\mathbf{w}^2)^T \mathbf{H}^2 \mathbf{w}^2 \leq \epsilon\} \quad (\text{D.2})$$

where \mathbf{H}^2 is the Hessian matrix of $\mathcal{L}(\mathbf{w}^1, \mathbf{w}^2)$ with respect to \mathbf{w}^2 .

Given that the sublevel set $S(\epsilon, \mathbf{w}^*) = \{\mathbf{w} \in \mathbb{R}^D : \frac{1}{2} \mathbf{w}^T \mathbf{H} \mathbf{w} \leq \epsilon\}$ is an ellipsoid body, which implies that \mathbf{H} is a positive definite matrix, it is evident that \mathbf{H}^2 is the principal submatrix of \mathbf{H} . Consequently, \mathbf{H}^2 is also a positive definite matrix, which implies that the sublevel set remains an ellipsoid.

D.2 Relationship between the Upper and Lower Bound

Theorem 6 (Eigenvalue Interlacing Theorem). *Suppose $\mathbf{A} \in \mathbb{R}^{n \times n}$ is symmetric, Let $\mathbf{B} \in \mathbb{R}^{m \times m}$ with $m < n$ be a principal submatrix (obtained by deleting both i -th row and i -th column for some values of i). Suppose \mathbf{A} has eigenvalues $\lambda_1 \leq \dots \leq \lambda_n$ and \mathbf{B} has eigenvalues $\beta_1 \leq \dots \leq \beta_m$. Then*

$$\lambda_k \leq \beta_k \leq \lambda_{k+n-m} \quad \text{for } k = 1, \dots, m \quad (\text{D.3})$$

And if $m = n - 1$,

$$\lambda_1 \leq \beta_1 \leq \lambda_2 \leq \beta_2 \leq \dots \leq \beta_{n-1} \leq \lambda_n \quad (\text{D.4})$$

Next, we provide an elucidation on the relationship between the upper bound and lower bound variations:

Lemma D.1. *The direct and straightforward relationship between the upper bound and the lower bound can be articulated as follows:*

1. *When the eigenvalues change, the upper and lower bounds will change in the same direction;*
2. *When the weight magnitude changes, the upper bound will change in the same direction as the upper bound or do not change.*

Proof.

1. When the eigenvalues change, the upper and lower bounds will change in the same direction;

By leveraging the Eigenvalue Interlacing Theorem (Theorem 6), the eigenvalues of the principal sub-matrix in the upper bound is bounded by the eigenvalues in the lower bound. It's obvious that if the eigenvalues in the lower bound change, the eigenvalues in the upper bound will also change in the same direction, leading to the upper and lower bounds will change in the same direction.

2. When the weight magnitude changes, the upper bound will change in the same direction as the upper bound or do not change.

It's noted that the number of weights in the lower bound is more than the one of weights in the upper bound. These weights are used to calculate the projection distance. So it's clear that when the weight magnitude changes, the upper bound will change in the same direction as the upper bound or not change.

D.3 Flatness & Lower Bound

We first introduce the definition of flatness, which is similar to the flatness definition in [PKA⁺21] and [GLC⁺23]:

Definition D.2. *Given a second-order derivable function $f(\mathbf{w}, \mathbf{x})$, where \mathbf{w} is the parameters and the \mathbf{x} is the input. Considering a hessian matrix \mathbf{H} w.r.t. parameters \mathbf{w} , the flatness of $f(\mathbf{w}, \mathbf{x})$ w.r.t. parameters is defined as the trace of \mathbf{H} , i.e. $\text{Tr}(\mathbf{H})$.*

As defined in definition D.2, a smaller trace indicates a flatter function. Next, we will provide the connection between the flatness and the lower bound:

Lemma D.3. *Given a well-trained neural network $f(\mathbf{w}, \mathbf{x})$, where \mathbf{w} is the parameters and the \mathbf{x} is the input. The lower bound of pruning ratio ρ_l and the flatness $\text{Tr}(\mathbf{H})$ obeys:*

$$\rho_l \leq 1 - \frac{\epsilon D}{\|\mathbf{w}^* - \mathbf{w}^k\|_2^2 \text{Tr}(\mathbf{H}) + \epsilon D} \quad (\text{D.5})$$

where \mathbf{H} is the hessian matrix of $f(\mathbf{w})$ w.r.t. \mathbf{w} , and $r_i = \epsilon/\lambda_i$ where λ_i is the eigenvalue of \mathbf{H} .

Proof.

$$\begin{aligned} \rho_l &= 1 - \frac{1}{D} \sum_{i=1}^D \frac{r_i^2}{\|\mathbf{w}^* - \mathbf{w}^k\|_2^2 + r_i^2} \\ &= 1 - \frac{\epsilon}{D} \sum_{i=1}^D \frac{1}{\|\mathbf{w}^* - \mathbf{w}^k\|_2^2 \lambda_i + \epsilon} \\ &\leq 1 - \frac{\epsilon}{D} \frac{D^2}{\sum_{i=1}^D (\|\mathbf{w}^* - \mathbf{w}^k\|_2^2 \lambda_i + \epsilon)} \quad \text{Cauchy-Schwarz Inequality.} \\ &= 1 - \frac{\epsilon D}{\|\mathbf{w}^* - \mathbf{w}^k\|_2^2 \sum_{i=1}^D \lambda_i + \epsilon D} \\ &= 1 - \frac{\epsilon D}{\|\mathbf{w}^* - \mathbf{w}^k\|_2^2 \text{Tr}(\mathbf{H}) + \epsilon D} \end{aligned}$$

It's obvious that if the trace of the hessian matrix becomes smaller, the lower bound will also decrease, indicating a higher sparsity level. Utilizing flatness as the optimization objective for network pruning is both a rational and efficacious approach.

Corollary D.4. Given a well-trained neural network $f(\mathbf{w}, \mathbf{x})$, where \mathbf{w} is the parameters and the \mathbf{x} is the input. The pruning ratio lower bound and the flatness obeys:

$$\rho_l \leq 1 - \frac{\epsilon D}{\|\mathbf{w}^* - \mathbf{w}^k\|_2^2 \text{Tr}(\mathbf{H}) + \epsilon D} \quad (\text{D.6})$$

where \mathbf{H} is the hessian matrix of $f(\mathbf{w}$ w.r.t. \mathbf{w} , and $r_i = \epsilon/\lambda_i$ where λ_i is the eigenvalue of \mathbf{H} . An informal version of this corollary can be stated as: flatness controls the pruning ratio lower bound, specifically a flatter neural network can be pruned more sparsely.

E Full Results

Here we present the full set of experiments performed for the results in the main text.

E.1 Small Weights Benefits Pruning

We verify that high flatness is not equal to high sparsity through hypothetical experiments. Considering that the hessian matrix of network A and network B_1, B_2, B_3, B_4 share eigenvalues $\{\lambda_1, \lambda_2, \dots, \lambda_n\}$, the weight magnitude of network B_1, B_2, B_3, B_4 is 2,3,4,5 times that of network A , we take the eigenvalues and weights from a FC network trained without regularization. In this way, the gap between the curves will be more obvious. For other networks, the trend of the curve gap is consistent, the prediction of the network pruning ratio is shown in the Figure. 7. It is observed from Figure. 7 that as the magnitude of network weights increases, the capacity of the network to tolerate pruning decreases. The pruning ratio threshold is affected not only by loss flatness but also the magnitude of weights. This finding, on the other hand, provides further evidence of the effectiveness of the l_1 -norm in pruning tasks.

E.2 Statistical Information of Weights in Various Experiments

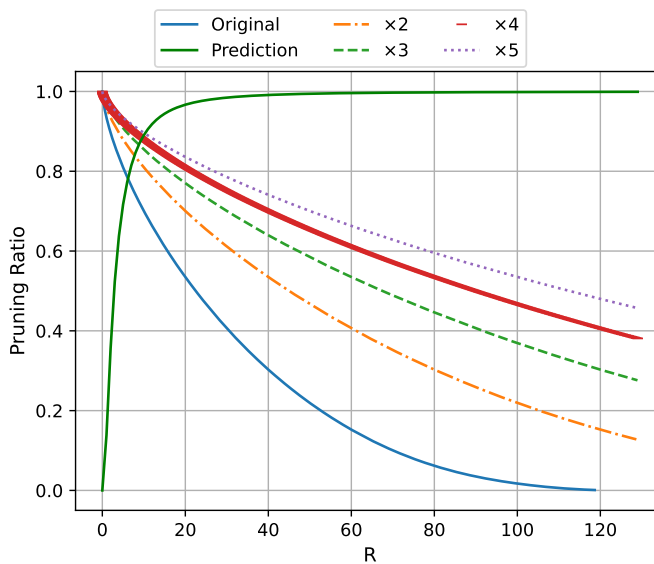


Figure 7: Pruning ratio prediction on different weight magnitude.

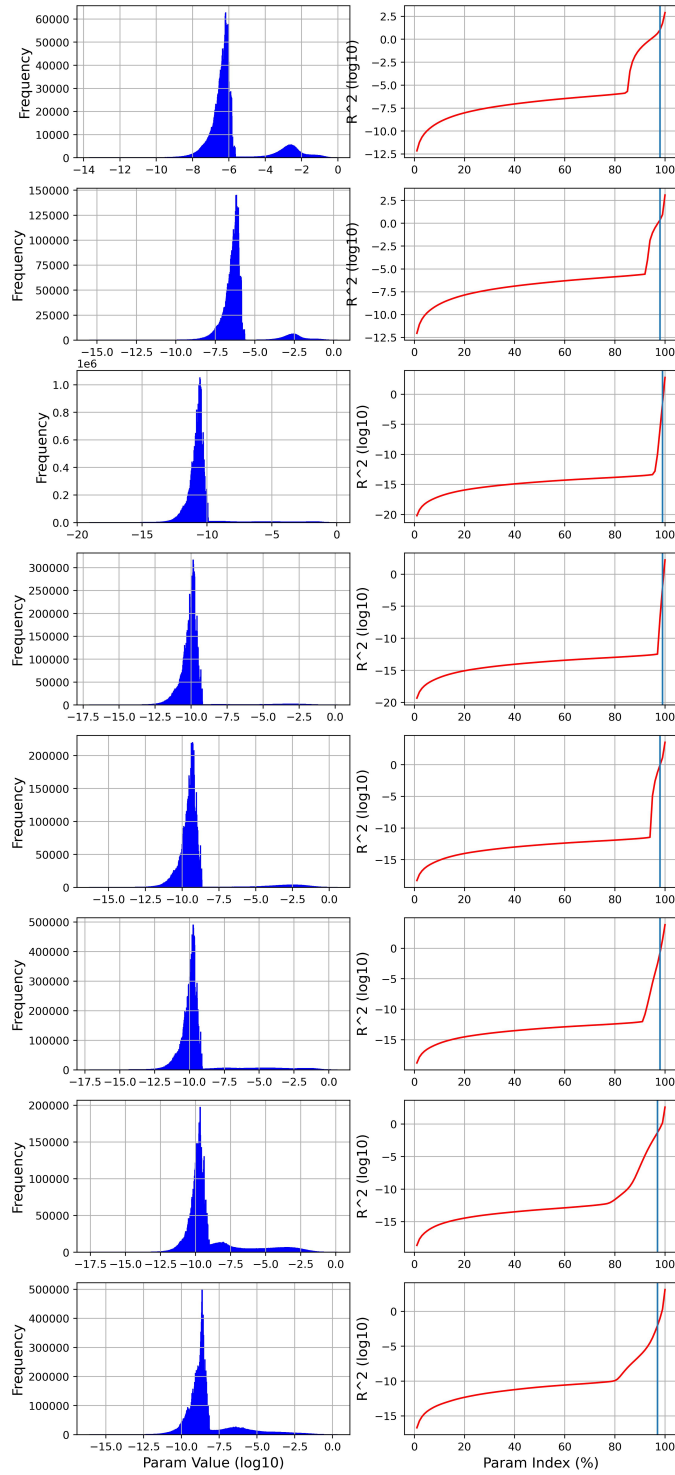


Figure 8: The same plots as Fig. 2(b) and Fig. 2(c) on CIFAR10 FC5,FC12,AlexNet,VGG16, and CIFAR100 ResNet18,ResNet50 and TinyImageNet ResNet18,ResNet50.